Chapter 4: The role of the molecular orbitals in predicting the reactivity and reaction pathways in alkene metathesis

4.1 Motivation

FMO theory showed promising potential for clarifying the cause for the difference in the activity of the main types of metal carbenes catalysts. To be able to do a fast screening of different catalysts we only looked at the initialisation steps of the reaction up to the formation of the metallacyclobutane. Hence, experimental cross metathesis reactions in the literature, each catalysed by one of the four metal carbenes, were selected for comparison with calculated results. The aim was to see if the FMO theory could be used to predict or explain known experimental results.

4.2 Article

The role of the molecular orbitals in predicting the reactivity and reaction pathways in alkene metathesis

Abstract

The Chauvin alkene metathesis mechanism for the homogeneous reactions of four different metal carbene catalysts has been studied theoretically using DFT. The frontier molecular orbital theory was applied to understand the factors that contribute to their reactivity as alkene metathesis catalysts. Geometry optimizations of all species were done at the GGA/PW91/DNP level and successive energy calculations at the B3LYP/LanL2DZ level. The results show that the location of the atomic orbital coefficients of the molecular orbital can be successfully used to predict the mechanistic pathway.

Keywords

Frontier orbitals, alkene metathesis, chemical reactivity, DFT

1. Introduction

Metal carbene complexes of especially ruthenium and molybdenum are efficient catalysts for alkene metathesis. After Chauvin proposed his mechanism in 1970 [1] several metal carbenes were tested for alkene metathesis activity. Among them four main types of metal carbenes can be seen, namely: Fischer-, Tebbe-, Grubbs- and Schrock-type metal carbenes (Fig. 1).

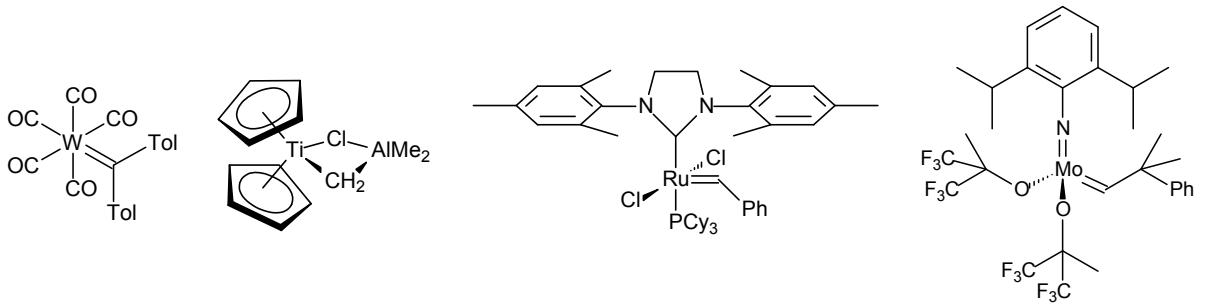

Fischer *Tebbe* *Grubbs* *Schrock*

Fig. 1. The metal carbenes chosen for the study.

The Fischer metal carbenes [2] were the first metal carbenes tested, but they showed poor alkene metathesis reactivity. Later Tebbe and co-workers [3] developed the Tebbe reagent which was the first catalyst to prove the Chauvin mechanism, because they were able to isolate the metallacyclobutane intermediate. However, it was only after the discovery of the Grubbs- [4] and Schrock-type [5] metal carbenes that high metathesis reactivity was observed.

Various approaches to the problem of identifying factors that contribute to the reactivity of the metal carbenes have been studied via molecular modeling. In several studies the electronic reaction profile of the alkene metathesis reaction was calculated and used as a source for elucidating experimental results [6-19]. These studies include the use of model catalysts, simplified alkenes and only consider part of the catalytic cycle. Only a few papers were published on true systems [20] and the complete catalytic cycle [21],[22]. Previously calculated electronic factors include the observation that for a Fischer-type carbene overlap occurs between the HOMO of the alkene and the LUMO of the metallocarbene [23]. Eisenstein and Hoffman [24] considered the orbital symmetry to be important as well as a more positively charged metal. This is supported by Cundari and Gordon [25] who also stated that the more positive the metal, the more active the catalyst for metathesis. For Grubbs-type metal carbenes, electronic factors also point to the key of alkene coordination to the catalyst. Vyboischchikov, Bühl and Thiel [26] found *trans* coordination of the alkene to L,

with $(L)Cl_2Ru=CH_2$ the active species, only allowed by frontier orbital overlap. Suresh and Koga [27] contributed orbital interaction in the transition state and metallacyclobutane to be responsible for the low barrier of the rate-determining step. Furthermore, Straub [28] ascribes the high activity of the second-generation Grubbs catalysts to electronic and steric stabilization of the active conformation of the carbene moiety by the NHC σ-donor ligand. In a later study Straub [29] investigated the effect of different ancillary ligands on the stabilization of the active conformation. A quantitative structure-activity relationship (QSAR) study was done on model 14-electron complexes, $LCl_2Ru=CH_2$, with 82 different dative ligands, L and ethylene as olefin by Occhipinti, Bjørsvik and Jensen [30]. They considered a host of electronic and steric effects based on their definition of productivity. Productivity was defined as the enthalpy difference between the inactive complex and the metallacyclobutane intermediate with respect to the active 14-electron complex [30]. Their model indicated that the best ligands are those that stabilize the high-oxidation state (+4) metallacyclobutane intermediate [30]. Lord *et al.* [31] considered the various bonding options with the metallacyclobutane because of possible ligand rotation by constructing the molecular orbital diagram. Fernández, Lugan and Lavigne [32] also probed the molecular orbitals for their possible stabilizing interaction in the metal carbene. Vasiliu *et al.* [33] calculated the bond energies in model Schrock metathesis catalysts to rationalize and understand their catalytic behavior. Both Folga and Ziegler [34] and Fox, Schofield and Schrock [35], investigated the electronic structure of Mo(VI) alkylidene complexes. The orbital interactions were considered to explain the occurrence of ligand rotation and the two possible pseudorotation routes for the formation of a square-pyramidal or trigonal-bipyramidal metallacyclobutane conformation.

Although several studies included the frontier orbitals as part of the explanation for the mechanism of alkene metathesis, no previous study, except work by the authors [36],[37], directly correlates the frontier orbitals to the activity of the metal carbenes as catalysts. Previously [36],[37] it was shown that the frontier molecular orbital (FMO) theory holds promise for predicting the alkene metathesis reactivity of metal

carbene catalysts. Results confirmed that the frontier orbital interaction of the catalyst-alkene coordination step is between the HOMO of the alkene and the LUMO of the catalyst. Furthermore, the location and contribution of AO to the LUMO of the metal carbenes can be used as chemical reactivity indicators for the alkene metathesis activation step and subsequent [2+2] cycloaddition reaction for the formation of the metallacyclobutane intermediate [37].

To further understand the frontier orbital interactions contributing to an active alkene metathesis catalyst the four reactions were investigated using molecular modeling. To understand their difference in metathesis reactivity the frontier orbitals and bonding molecular orbitals of the mechanistic steps were investigated from the reagents (**A1** or **D1**), through the transition state, to the formation of the metallacyclobutane intermediate (**A3** or **D3**) (**Fig. 2**).

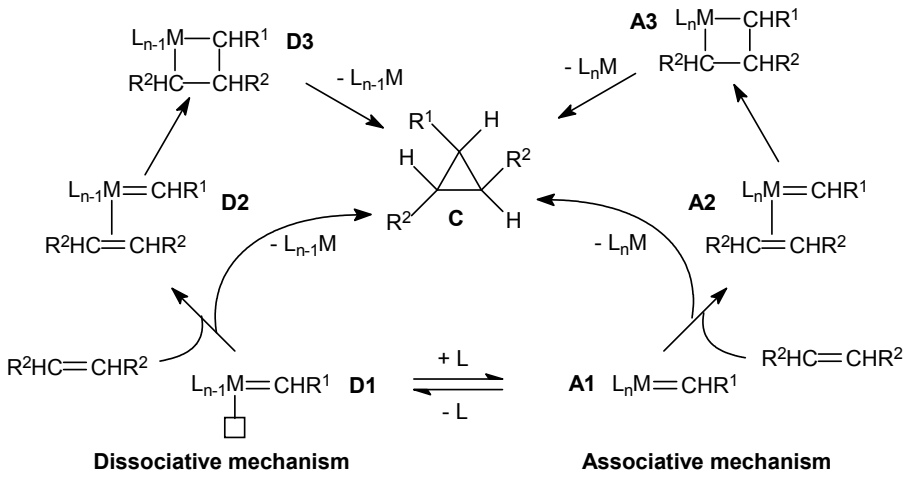

Fig. 2. Part of the general alkene metathesis mechanism to show the associative and dissociative mechanistic pathways for the formation of the metallacyclobutane intermediate.

The following aspects of the FMO theory [38] were used as criteria to assess the reactivity of the metal carbene catalysts: In the transition state the carbon atoms of the alkene coordinates sequentially to the catalyst. Where will this primary overlap and

consecutive secondary overlap of the HOMO with the LUMO orbitals occur on the metal carbene? (Fig. 3)

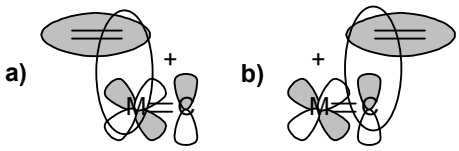

Fig.3. Two possible primary overlap options according to the AO coefficients for a) formation of metathesis products and b) cyclopropanation.

In the transition state and metallacyclobutane will the bonding orbitals lead to the next step or do they indicate the formation of a different product than the expected product? (Fig. 4) How deep does the bonding orbital lie in the MO diagram? Does it indicate a stable bond? Is it the lowest energy bond? Between the two possible reagents that can bond first, which one has the biggest overlap between the HOMO and the LUMO orbitals? Does the energy profile of the reaction give us any more clues to the reactivity and does it correlate with the FMO theory? This chapter is an in-depth study of the viability of using the FMO theory to predict the reactivity of metal carbenes as alkene metathesis catalysts. To that end literature reactions [39-42] were chosen of the four main types of metal carbene catalysts. Due to a lack of cross metathesis reactions reported in literature, four types of reactions with the same substrate but with different catalyst species could not be found.

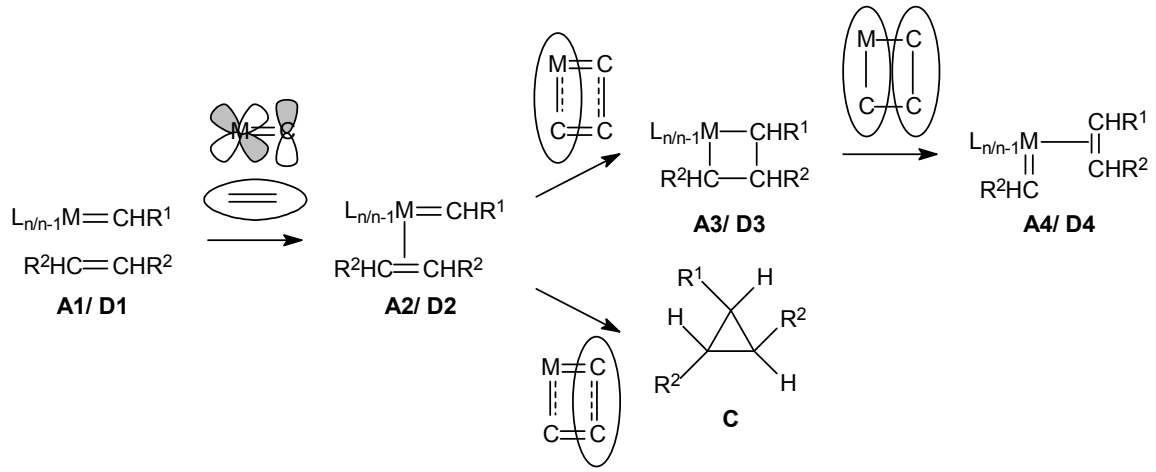

Fig.4. The orbital overlaps of each step that will lead to the formation of the next step.

Therefore, for the study the reactions between: 1-pentene with (**W(Tol)_cat**) as catalyst [39], isobutene and methylenecyclohexane with (**Tebbe_cat**) as catalyst [40], allylbenzene and an allylic alcohol with (**Gr2_cat**) as catalyst [41], and styrene and *n*-hexyl with (**Mo(Ph)**) as catalyst [42] were chosen (Table 1).

Table 1 A summary of the cross metathesis reactions of the four metal carbenes chosen for this study

Catalyst	Alkene(s)	Product(s)	Ref
W(Tol)_cat	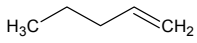	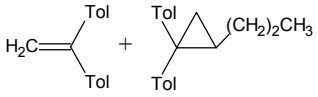 36% 27%	[39]
	[Reaction conditions: at 70°C for 3.25h]		
Tebbe_cat	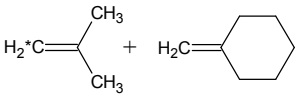	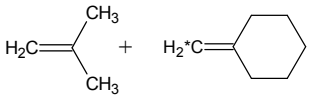	[40]
	[Reaction conditions: at 52°C for 30h]		
Gr2_cat	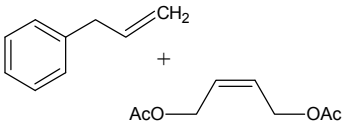	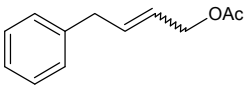 80%	[41]
	[Reaction conditions: at 40°C for 12h]		
Mo(Ph)	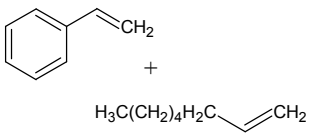	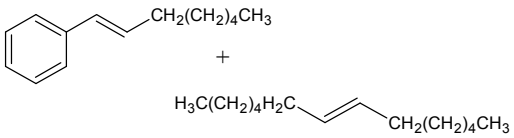 89% 2%	[42]
	[Reaction conditions: at 25°C for 1h]		

By comparing each step of the chosen mechanism part with the same step of a different carbene, the importance of the frontier orbitals will be elucidated. The reaction pathways are shown in Fig. 5-8. The reaction states where the structure is shown were calculated.

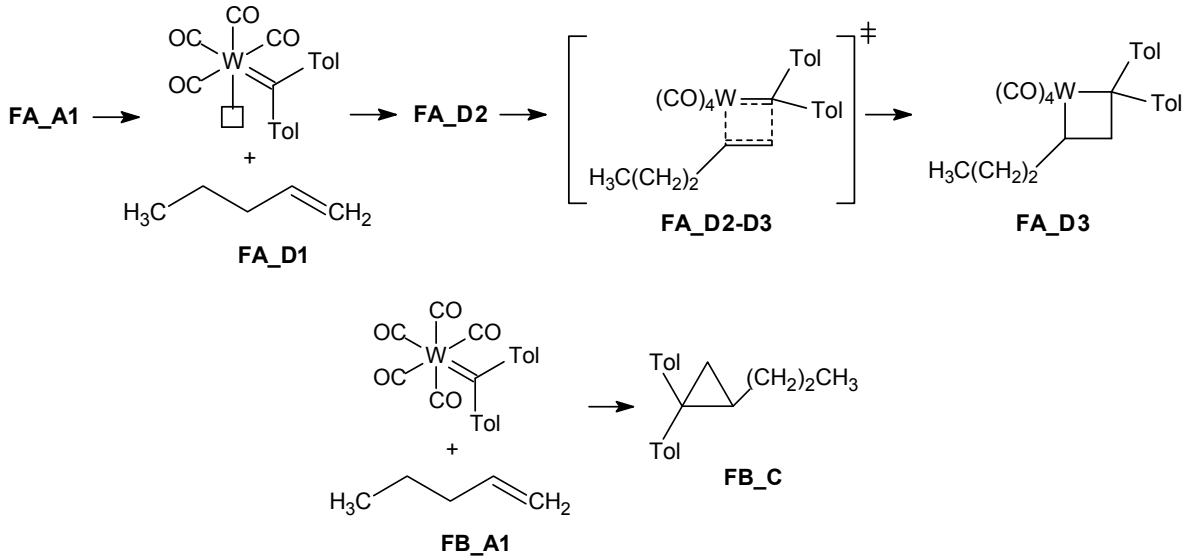

Fig. 5. The two possible pathways (**FA** and **FB**) for the reaction of pentene with Fischer carbene as catalyst.

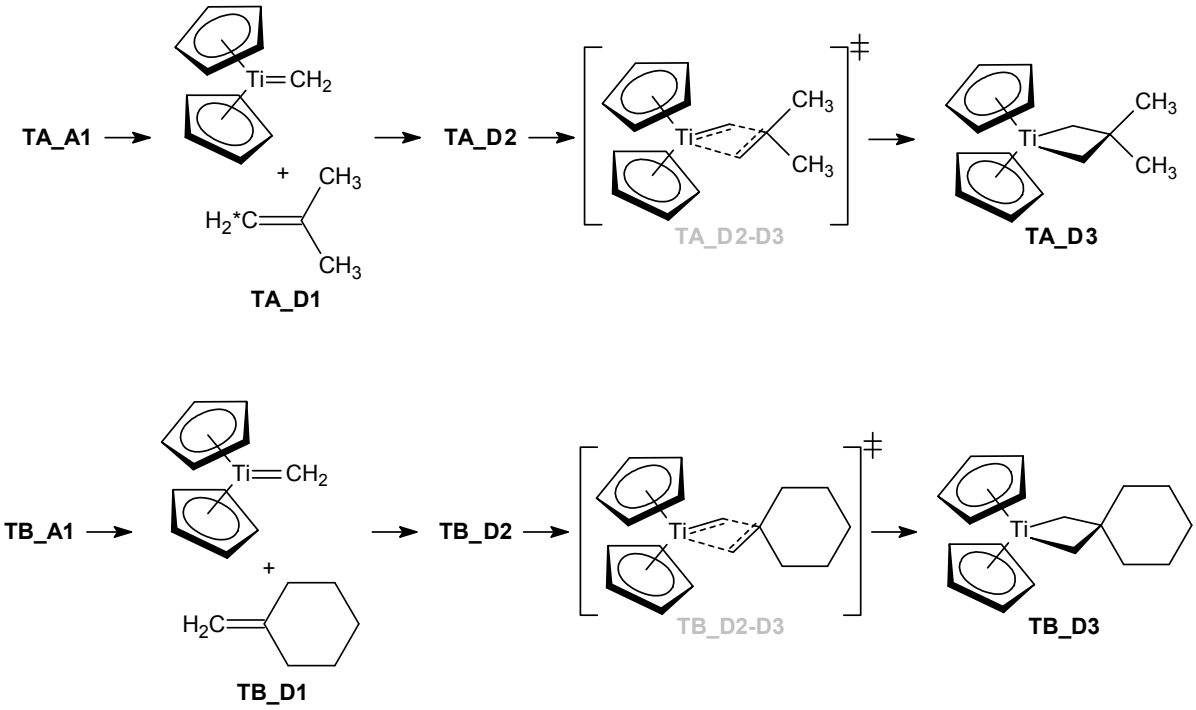

Fig. 6. The two possible pathways (**TA** and **TB**) for the reaction of reagent A and reagent B with Tebbe carbene as catalyst.

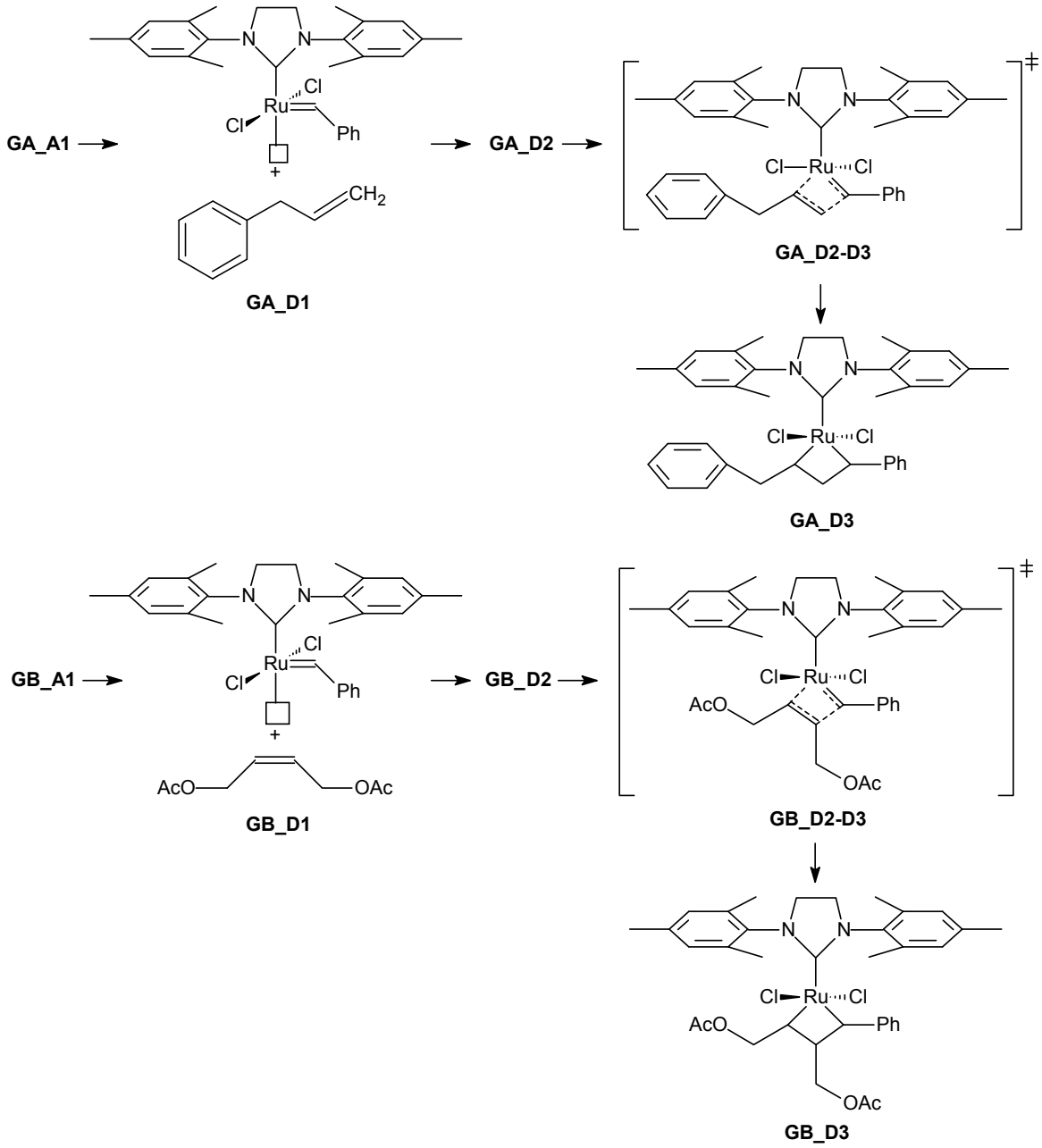

Fig. 7. The two possible pathways (**GA** and **GB**) for the reaction of reagent A and reagent B with Grubbs carbene as catalyst.

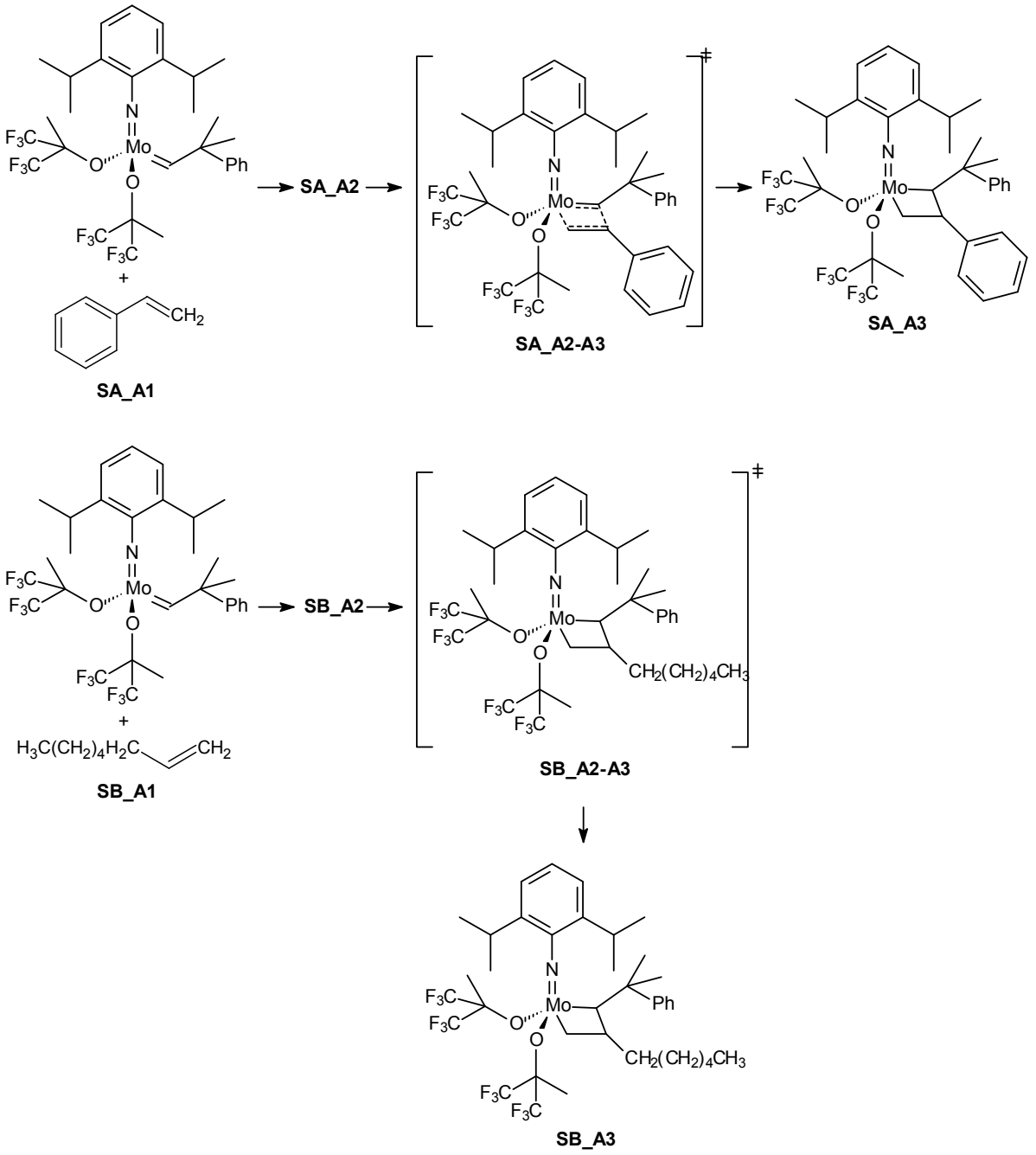

Fig. 8. The two possible pathways (**SA** and **SB**) for the reaction of reagent A and reagent B with Schrock carbene as catalyst.

2. Method

The initial geometry optimization of each reaction state, and the potential-energy surface (PES) scan to locate the transition state, were done with the DMol^3 DFT module of Materials Studio 5.5 [43]. The GGA PW91 functional with the DNP basis set was selected as the calculation method. The molecular orbitals (MO) were

calculated from the DMol^3 optimized structures with Gaussian 03 [44] by using the B3LYP functional with the LanL2DZ basis set. 2D visualization of the MOs was done with Chemissian [45]. The 3D structures of the molecules were drawn with the ORTEP [46] drawing software.

For each reaction state the LUMO and HOMO were calculated. The results show the orbital picture with an isovalue of 0.55, a 2D plane through the orbital, the atomic orbital coefficients of the molecular orbital and the coordination key of the molecule. The atoms used to define the plane are shaded in grey in the ORTEP drawings of the molecules. The coordination key of the internal axis of the molecule in Gaussian is given, because a different internal axis for each molecule is defined by Gaussian. Thus to be able to compare the orientation of the molecules at the double bond the internal axis must be taken into account and the orbital labels transposed according to the user-defined axis.

Only the bonding orbitals where the metal atom, the carbene carbon atom and the two carbon atoms of the double bond of the alkene have an atomic orbital coefficients (AOC) contribution of ≥ 0.20 were investigated.

3. Results and Discussion

3.1 Fischer-type metal carbene

Two pathways for the reaction of 1-pentene with **W(Tol)_cat** as catalyst are possible: the dissociative pathway that leads to potential formation of metathesis products (**FA_D1**) or the associative pathway that leads to cyclopropanation (**FB_A1**) (Fig. 5). In all figures hydrogen atoms are omitted for clarity.

In the **FA_D1** reaction state (Fig. 9) the primary overlap of the HOMO of 1-pentene with the LUMO of the catalyst will occur at the **C**C-atom. This will happen because of the bigger atomic orbital coefficient (AOC) on the **C**C-atom (0.45) than the **W**-atom (0.21). The orientation of the AO on the **C**C-atom also allows this overlap to

take place, because of the correlation with the orientation of the MO of the **CA1**- and **CA2**-atoms. To this extent, the expected product formation will be cyclopropanation. In reaction state **FA_D2-D3** (Fig. 10), the transition state, it can be seen that both the metathesis and cyclopropanation products pathway are possible. In both cases there is a bonding orbital present in the molecule with overlap, in the one case between the **W**- and **CA2**-atoms, and in the other case between the **CC**- and **CA1**-atoms. The lowest-energy-bonding orbital indicates the strongest bond thus the preferred product pathway, which in this case is the HOMO-47 for the cyclopropanation. Along the metathesis pathway in the next reaction state (**FA_D3**) (Fig. 11) the calculations show more unstable high energy bonding orbitals close to the HOMO of the molecule. The correct orbital overlap is present for the following rearrangement of the double bond to the metathesis product.

For the associative pathway in reaction state **FB_A1** (Fig. 12) the primary overlap will clearly be at the **CC**-atom leading to the orbital arrangement that relates to the direct formation of a cyclopropane ring. The AOC on the **CC**-atom is 0.49 as opposed to the AOC on the **W**-atom of 0.18. When we look at the lowest-energy bonding orbital in the cyclopropane ring (**FB_C**) (Fig. 13), the three carbon atoms forming the ring are closely bonded to each other and the cyclopropanation product is stable.

FA_D1

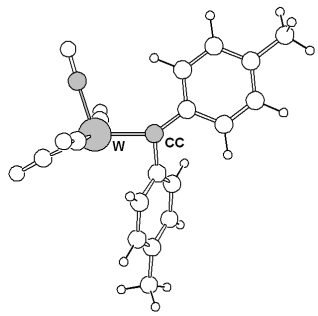

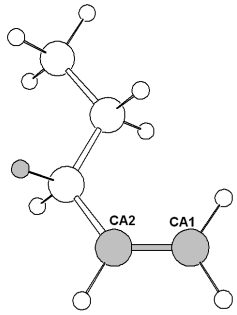

LUMO HOMO

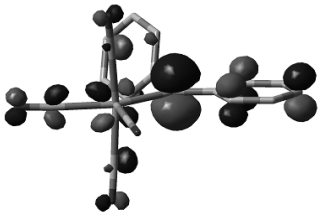

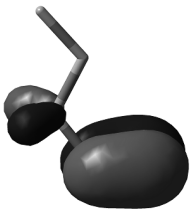

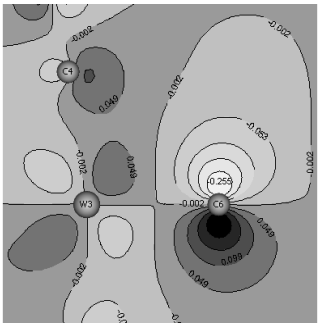

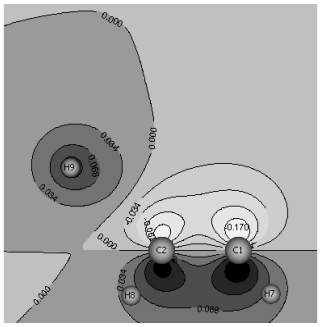

Atom	AO	|coefficient|	Atom	AO	|coefficient|
CC	p_z	0.45	CA1	p_z	0.49
CC	p_z	0.28	CA2	p_z	0.44
W	d_{xz}	0.21	CA1	p_z	0.21

Coordination key:

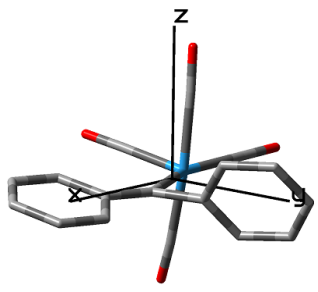

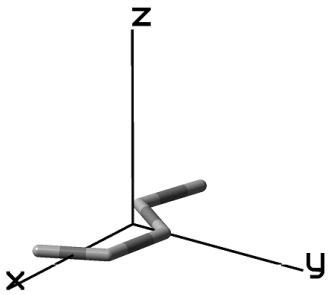

Fig. 9. Reaction state **FA_D1.**

FA_D2-D3

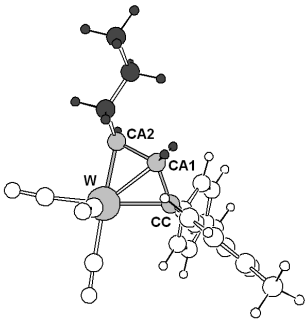

HOMO HOMO-3 HOMO-47



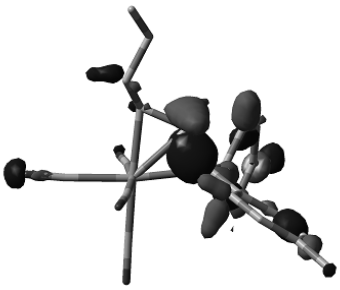
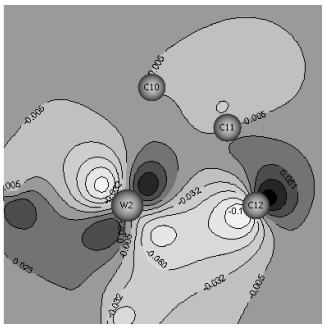
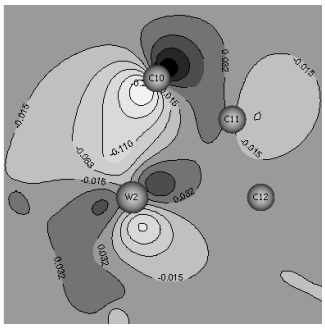
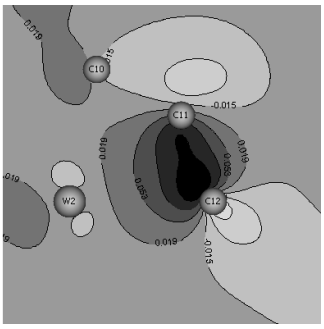

Atom	AO	|coefficient|	Atom	AO	|coefficient|	Atom	AO	|coefficient|
W	d_{xy}	0.39	CA2	p_z	0.39	CC	p_x	0.21
CC	p_z	0.21	W	d_{xz}	0.26	CA1	p_z	0.20
			CA2	p_z	0.24			

Coordination key:

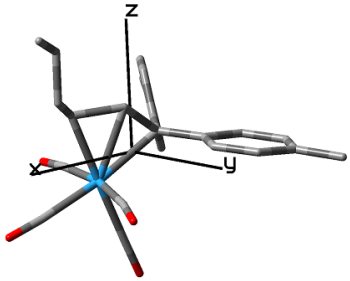

Fig. 10. Reaction state **FA_D2-D3.**

FA_D3

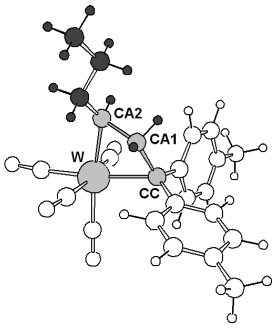

HOMO HOMO-3

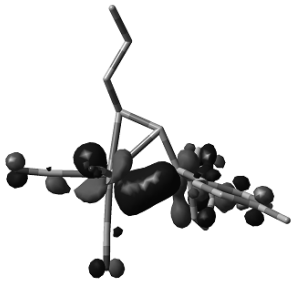

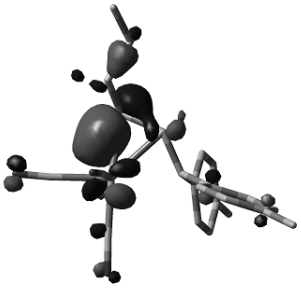

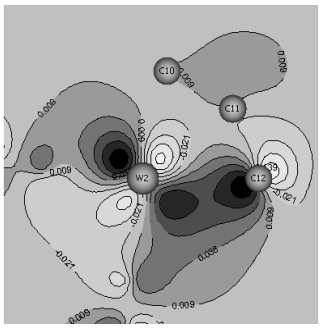

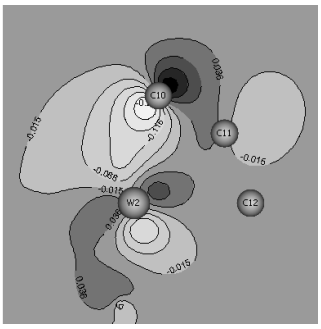

Atom	AO	|coefficient|	Atom	AO	|coefficient|
W	$d_{x^2-y^2}$	0.31	CA2	p_z	0.42
CC	p_z	0.22	CA2	p_z	0.28
W	$d_{z^2-r^2}$	0.21	W	d_{xz}	0.27

Coordination key:

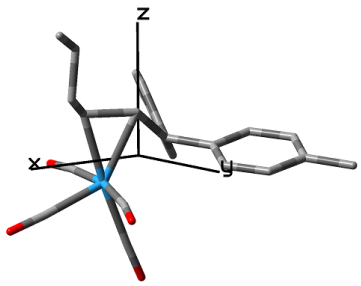

Fig. 11. Reaction state **FA_D3.**

FB_A1

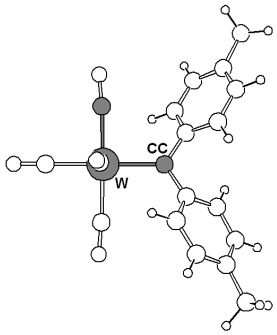

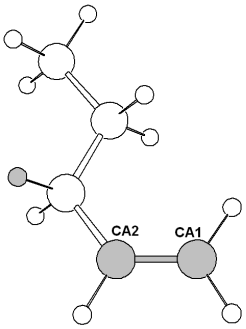

LUMO HOMO

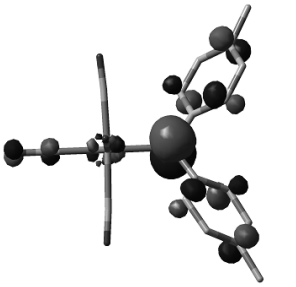

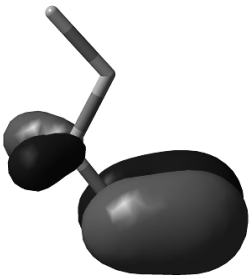

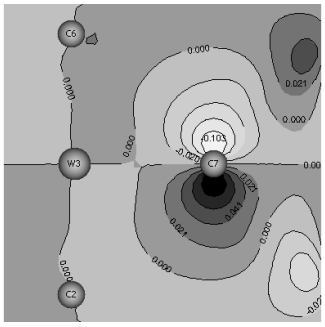

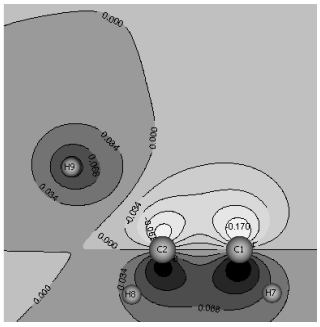

Atom	AO	|coefficient|	Atom	AO	|coefficient|
CC	p_z	0.49	CA1	p_z	0.49
CC	p_z	0.26	CA2	p_z	0.44
W	d_{xz}	0.18	CA1	p_z	0.21

Coordination key:

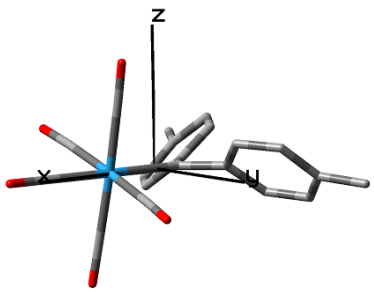

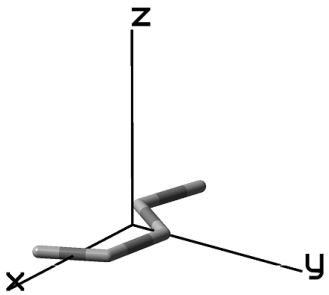

Fig. 12. Reaction state **FB_A1.**

FB_C

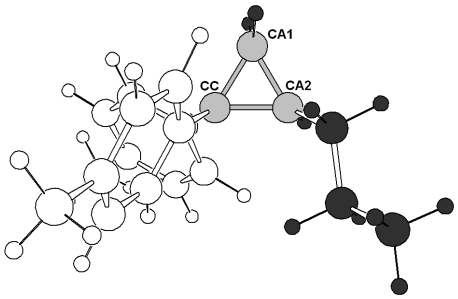

HOMO-4 HOMO-5 HOMO-7 HOMO-32

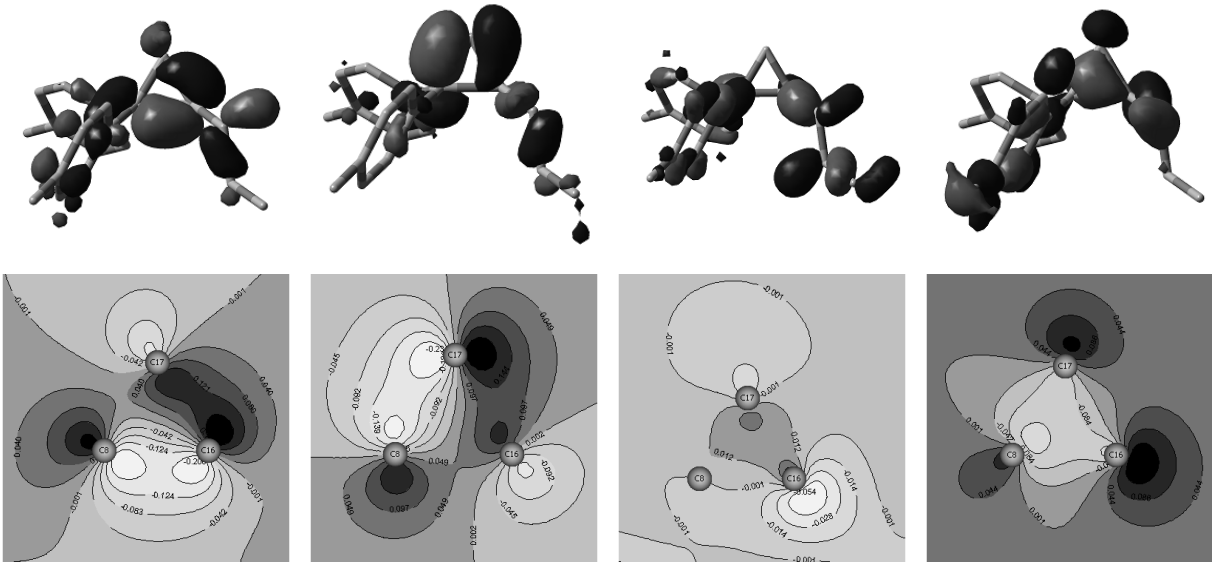

Atom	AO	|coefficient|	Atom	AO	|coefficient|	Atom	AO	|coefficient|	Atom	AO	|coefficient|
CA2	p_z	0.29	CA1	p_y	0.40	CC	p_x	0.23	CA2	p_y	0.23
CC	p_y	0.27	CC	p_z	0.34	CA2	p_x	0.22	CA1	p_z	0.20
CA1	p_z	0.21	CA2	p_z	0.21						
CA2	p_y	0.20									

Coordination key:

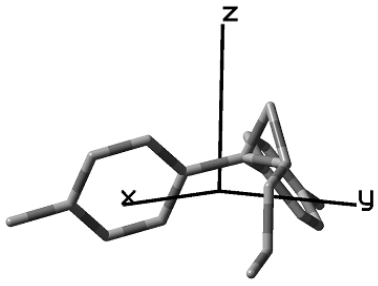

Fig. 13. Reaction state **FB_C.**

The reaction energy profiles of the two possible pathways can be seen in Fig. 14. In Fig. 15 the partial molecular orbital energy diagram of the bonding MOs contributing to the formation of metathesis products of the individual reaction steps are shown. The orbital gap value $|E_H\text{-}E_L|$ denotes the difference between the HOMO energy of the alkene and the LUMO energy of the catalyst. Only the HOMO, LUMO and bonding molecular orbitals with atomic orbital coefficients of the metal and carbene carbon atoms and alkene carbon atoms larger than |0.2| are included in the diagram. The reaction **FB** has the lower-energy pathway and will lead to the most favored product, thus cyclopropanation. This is also supported by the results of the orbital energy diagram. In both states **FA_D2-D3** and **FB_C** the lowest bonding orbital is the formation of a cyclopropane ring via the AO overlap of the **CC**-, **CA1**- and **CA2**-atoms. The bonding orbitals indicating the formation of metathesis products have a higher energy than the original HOMO energy and are thus more unstable and less likely to lead to the expected metathesis product formation. The orbital gap value $|E_H\text{-}E_L|$ of reaction FB is also smaller indicating the biggest overlap and the strongest bond.

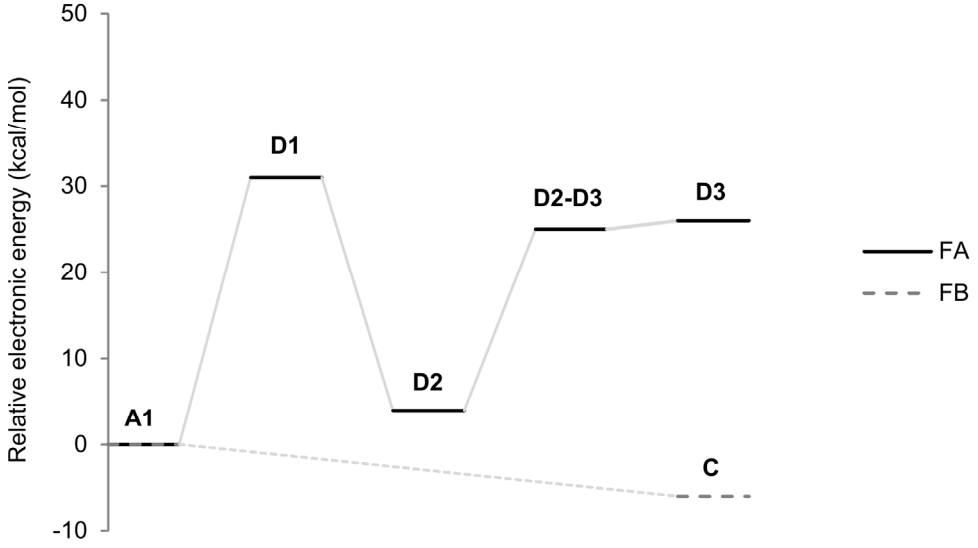

Fig. 14. Relative electronic energy (kcal/mol) reaction profile of alkene(s) with Fischer carbene.

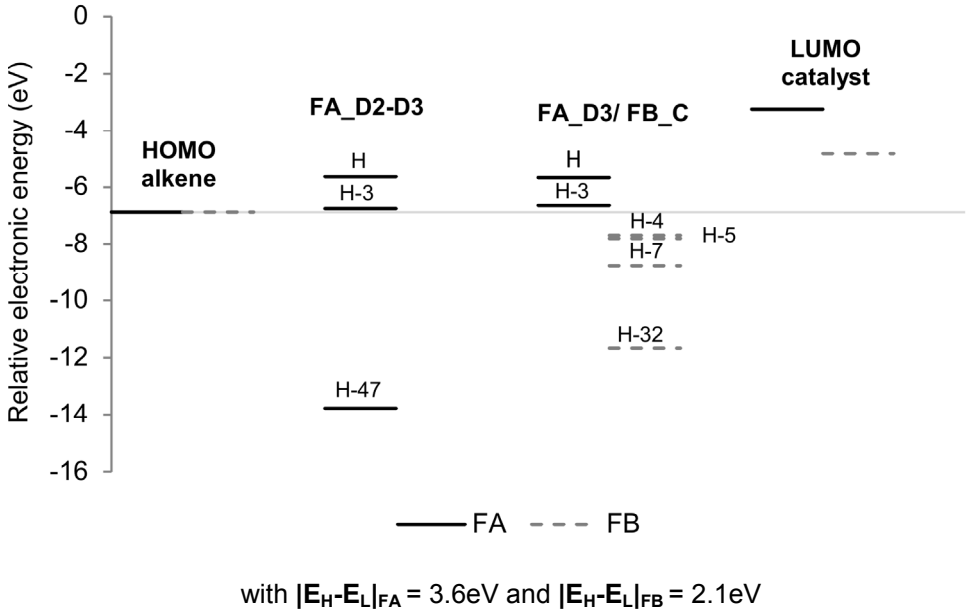

Fig. 15. Partial MO diagram of the bonding MOs of the Fischer catalyzed reaction.

In the experimental reaction of 1-pentene with a Fischer carbene as catalyst [39] the reaction ran for 3.25 hours at 70°C. The product yield was the formation of 36% metathesis products and 27% cyclopropanation (Table 1). In the modelling results the calculations indicate that a cyclopropane ring will form as the major product. If we take into account the difference of the experimental reaction conditions from the calculated modelling conditions (in vacuum at 1atm), as well as the limited number of reaction steps calculated, the high experimental reaction temperature can cause the formation of slightly more metathesis products. Overall there is a clear indication in the modelling of the weak metathesis reactivity of Fischer metal carbenes as catalysts of the reaction.

3.2 Tebbe-type metal carbene

After dissociation of the $AlMe_3$-ligand only the CH_2 group is left as part of the newly formed metal carbene. The metal carbene double bond, especially the **Ti**-atom is greatly shielded by the ligand rings. Calculations of the transition states of the **TA** and **TB** reactions both failed to give a maximum. The metallacyclobutane intermediates' metal bond lengths are also slightly elongated from under the ligand rings. The

primary orbital overlap in both the **TA**- and **TB** reaction will occur at the **Ti**-atom, because of a complete absence of AOC on the CC-atom (**TA_D1** and **TB_D1**) (Fig. 16 and Fig. 18). Even though the size of the AOC on the **Ti**-atom is big (0.76) the lowest-energy bonding orbitals in both reactions states **TA_D3** and **TB_D3** (Fig. 17 and Fig. 19) are the bonding between the **CC**-, **CA1**- and **CA2**-atoms. The product formation will lead away from the expected metathesis products to cyclopropanation [47].

TA_D1

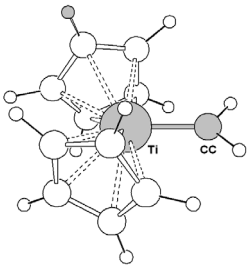

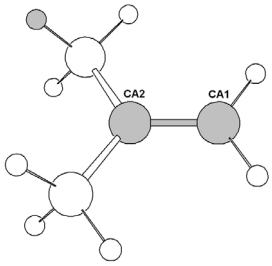

LUMO HOMO

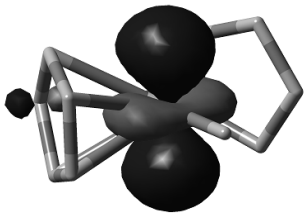

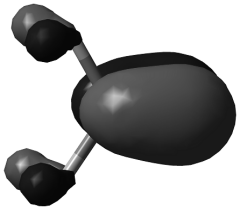

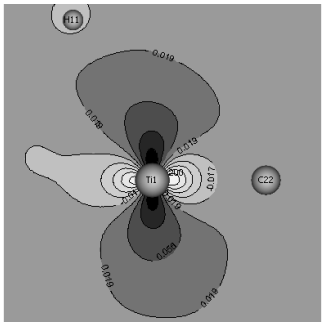

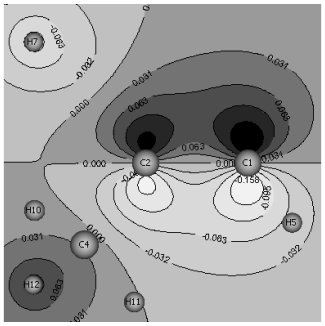

Atom	AO	|coefficient|	Atom	AO	|coefficient|
Ti	$d_{z^2-r^2}$	0.72	CA1	p_z	0.50
Ti	$d_{z^2-r^2}$	0.28	CA2	p_z	0.44
			CA1	p_z	0.22

Coordination key:

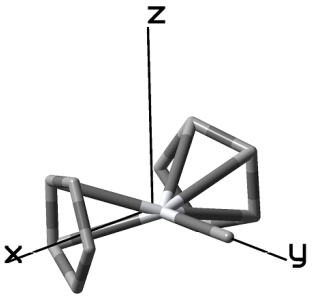

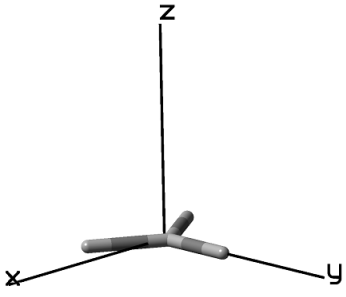

Fig. 16. Reaction state **TA_D1.**

TA_D3

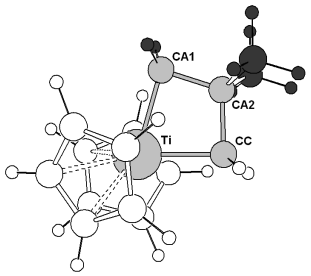

HOMO HOMO-2 HOMO-6 HOMO-10

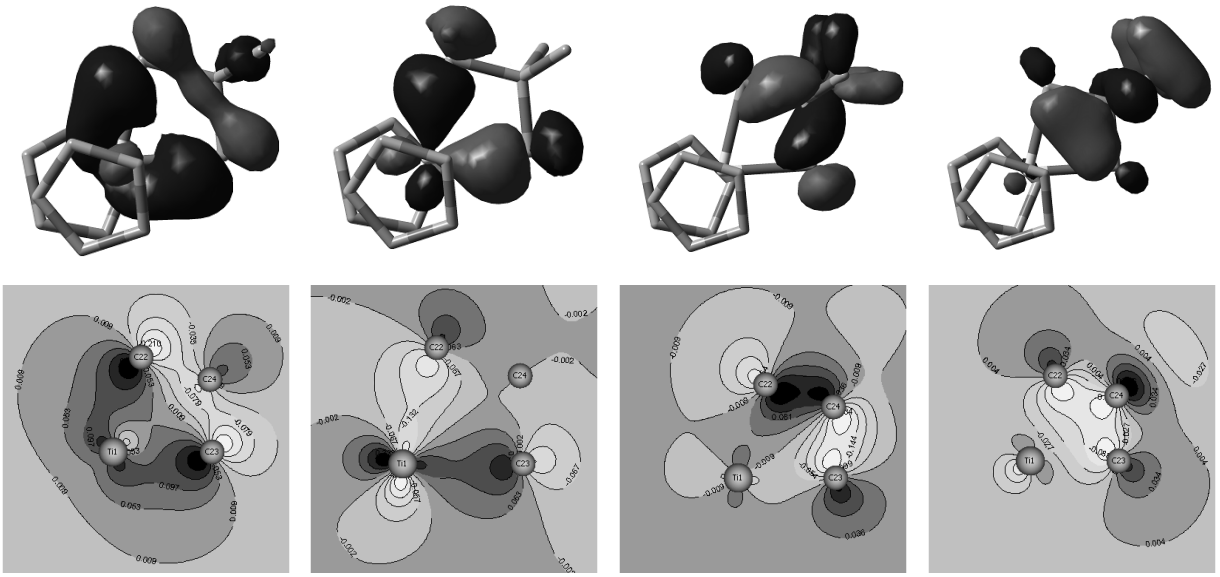

Atom	AO	|coef-ficient|	Atom	AO	|coef-ficient|	Atom	AO	|coef-ficient|	Atom	AO	|coef-ficient|
CC	p_x	0.38	Ti	d_{xz}	0.43	CA2	p_z	0.39	CA2	p_x	0.28
CA1	p_x	0.38	CA1	p_x	0.33	CA1	p_z	0.31	CC	p_z	0.20
Ti	$d_{z^2-r^2}$	0.27	CC	p_x	0.33	CC	p_z	0.31	CA1	p_z	0.20
Ti	$d_{x^2-y^2}$	0.24									
CA2	p_x	0.22									
CC	p_x	0.20									
CA1	p_x	0.20									

Coordination key:

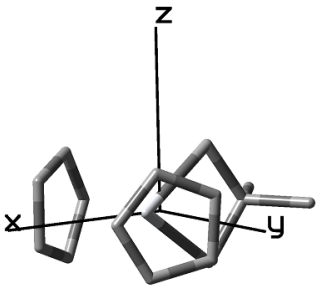

Fig. 17. Reaction state **TA_D3.**

TB_D1

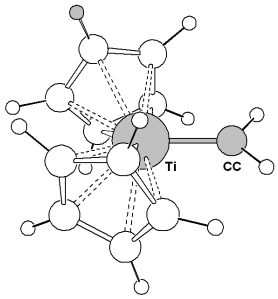

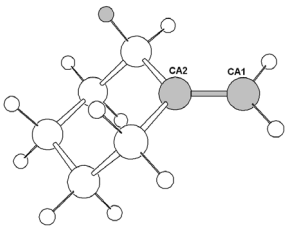

LUMO HOMO

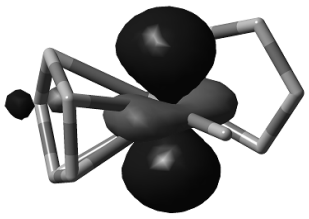

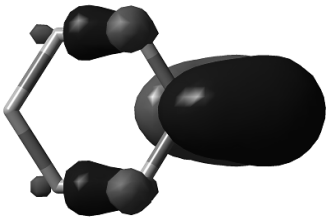

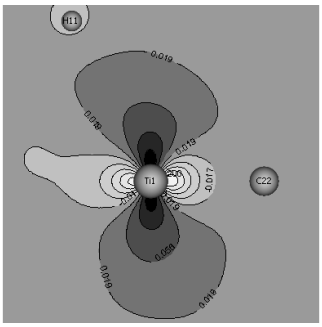

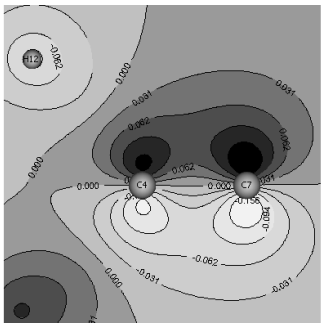

Atom	AO	|coefficient|	Atom	AO	|coefficient|
Ti	$d_{z^2-r^2}$	0.72	CA1	p_z	0.46
Ti	$d_{z^2-r^2}$	0.28	CA2	p_z	0.38
			CA1	p_z	0.21

Coordination key:

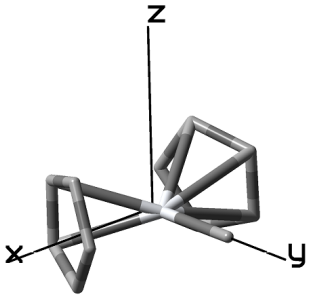

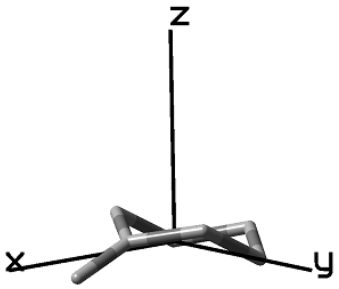

Fig. 18. Reaction state **TB_D1.**

TB_D3

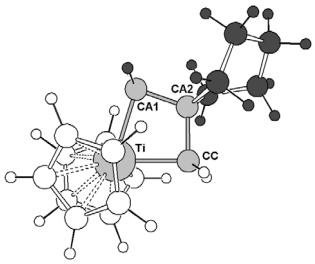

HOMO HOMO-2 HOMO-7

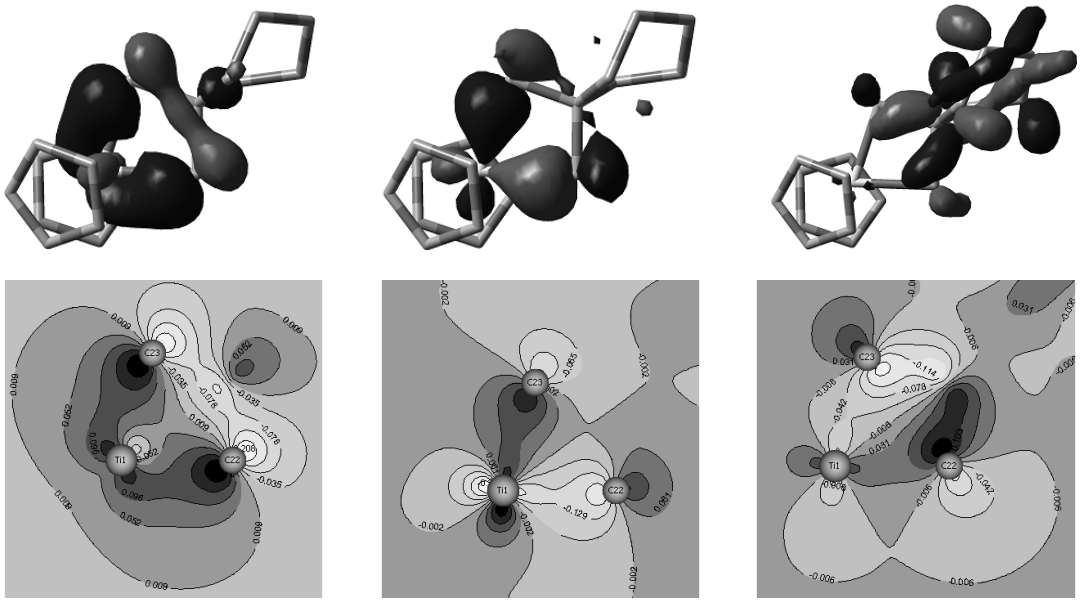

Atom	AO	|coefficient|	Atom	AO	|coefficient|	Atom	AO	|coefficient|
CC	p_x	0.38	Ti	d_{xz}	0.43	CA2	p_z	0.24
CA1	p_x	0.37	CA1	p_x	0.33	CA1	p_z	0.23
Ti	$d_{z^2-r^2}$	0.28	CC	p_x	0.33	CC	p_z	0.23
Ti	$d_{x^2-y^2}$	0.23						
CA2	p_x	0.22						
CC	p_x	0.20						
CA1	p_x	0.20						

Coordination key:

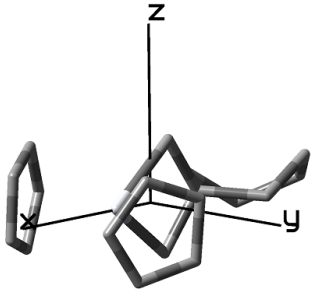

Fig. 19. Reaction state **TB_D3.**

In both reactions the reaction energy profiles (Fig. 20) are very similar with the **TA** metallacyclobutane (**D3**) slightly lower in energy. The bonding orbitals (Fig. 21) leading to possible formation of metathesis are slightly higher in energy than the original HOMO energy. The bonding orbitals leading to possible formation of a cyclopropane ring are lower in energy and more stable. The **TA** reaction is clearly more favored. The orbital gap value $|E_H\text{-}E_L|$ is the same (4.5eV) for both **TA** and **TB**.

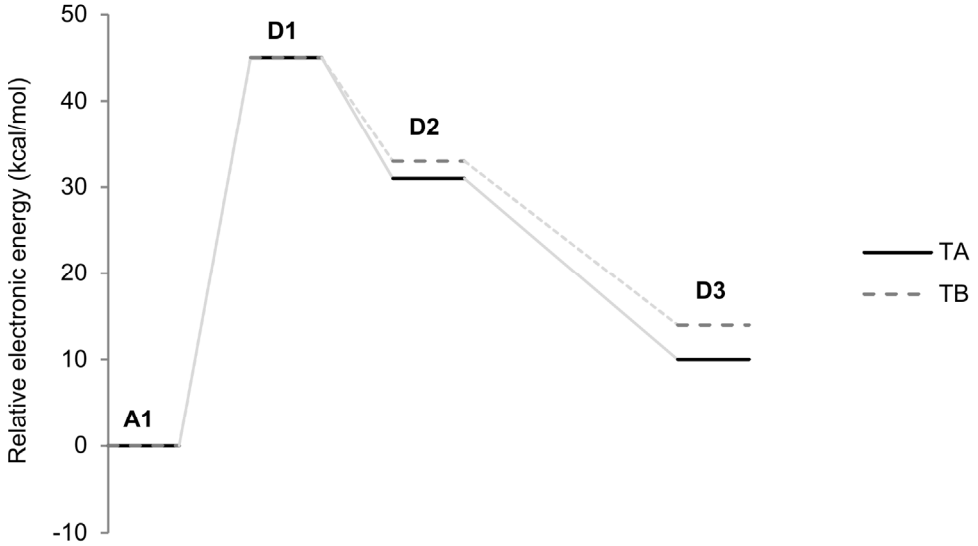

Fig. 20. Relative electronic energy (kcal/mol) reaction profile of alkene(s) with Tebbe carbenes.

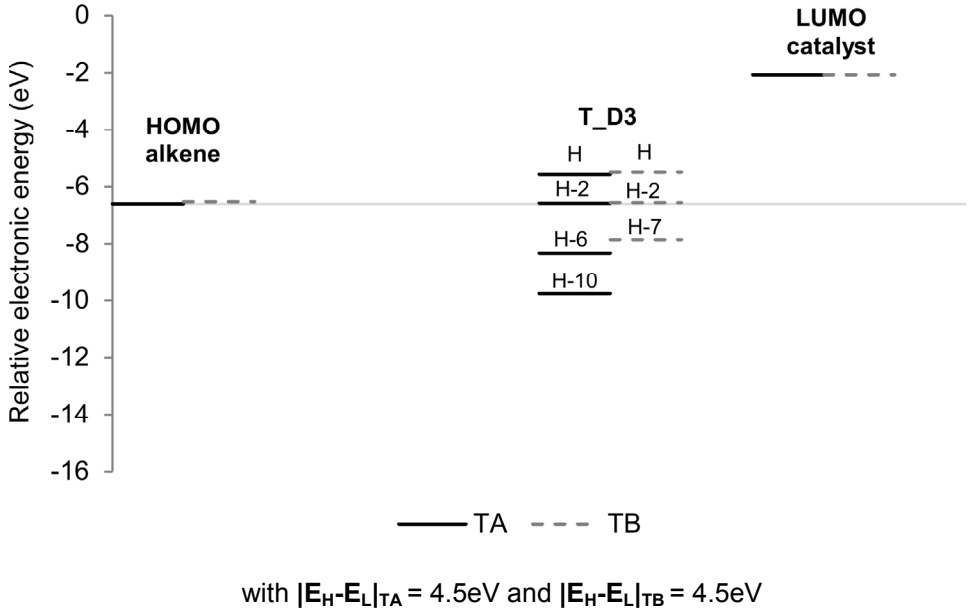

Fig. 21. Partial MO diagram of the bonding MOs of the Tebbe catalyzed reaction.

Experimentally the reaction of isobutene and methylenecyclohexane with **Tebbe_cat** as catalyst [40] ran for 30 hours at 52°C in which time the metathesis products formed. The reaction temperature correlates with the high activation energy needed for the dissociation of the $AlMe_3$-ligand. From the long reaction runtime needed to form metathesis products it is also apparent that the **Tebbe_cat** is not a good metathesis catalyst. The Tebbe reagent has also proved by modeling to be a difficult and weak catalyst.

3.3 Grubbs-type metal carbene

One of the metathesis catalysts that show very high reactivity is the **Gr2_cat** [4]. In reaction state **GA_D1** (Fig. 22) and **GB_D1** (Fig. 25) the primary overlap of the HOMO of the alkene with the LUMO of the catalyst will take place at the **Ru**-atom (AOC 0.44) to form the transition state leading to the formation of metathesis products. There also is secondary overlap possible at the **C**C-atom (AOC 0.37) for the consecutive formation of the metallacyclobutane intermediate. The orientation and accessibility of the LUMO allows the easy overlap of the HOMO. The transition states, **GA_D2-D3** (Fig. 23) and **GB_D2-D3** (Fig. 26) have lower-energy bonding orbitals with the overlap between the **Ru**-atom and the **CA2**-atom in both cases to indicate the formation of the metallacyclobutane intermediate. In the reaction state **GA_D3** (Fig. 24), the bonding orbitals point to the formation of metathesis products. The **HOMO-15** and **HOMO-18** orbitals will lead to the new catalyst in the catalytic cycle and the **HOMO-36** and **HOMO-59** to the first new alkene. For the **GB_D3** (Fig. 27) reaction state, only one bonding orbital shows the possible formation of metathesis products.

GA_D1

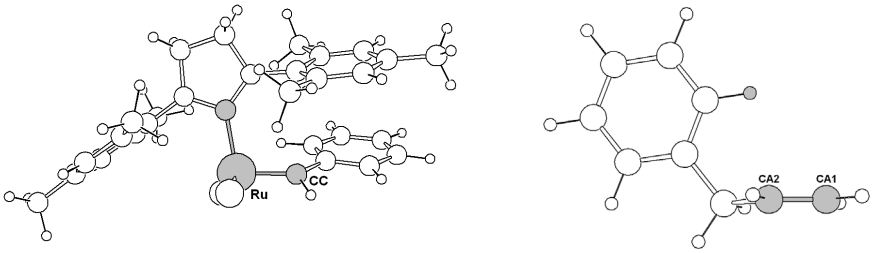

LUMO HOMO-2

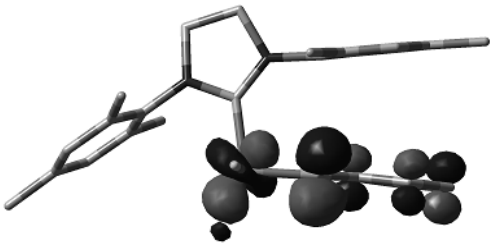

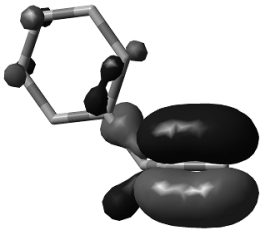

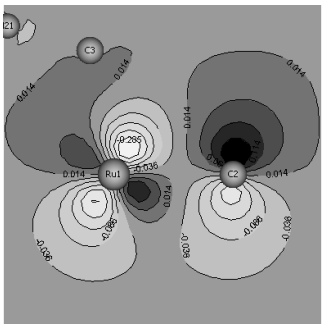

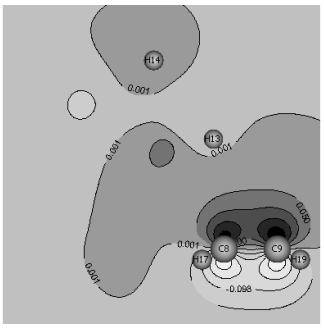

Atom	AO	|coefficient|	Atom	AO	|coefficient|
Ru	d_{xy}	0.44	CA2	p_y	0.37
CC	p_y	0.37	CA1	p_y	0.36
CC	p_y	0.26	CA1	p_x	0.26
Ru	d_{yz}	0.21	CA2	p_x	0.22

Coordination key:

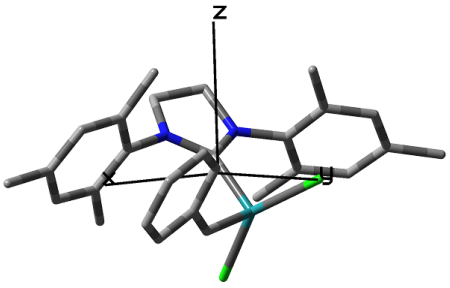

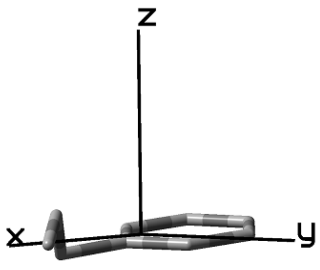

Fig. 22. Reaction state **GA_D1.**

GA_D2-D3

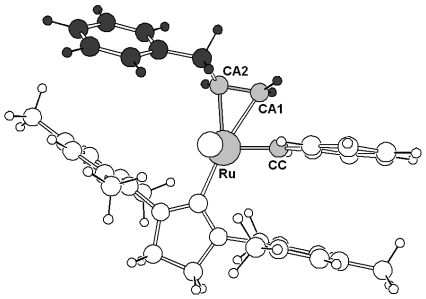

HOMO-14

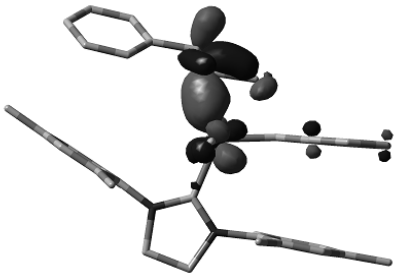

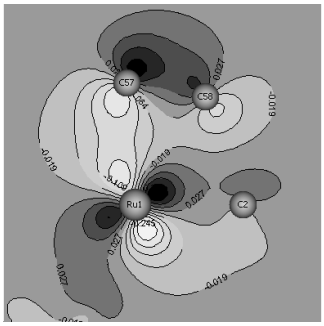

Atom	AO	|coefficient|
Ru	d_{xy}	0.37
CA2	p_y	0.26
CA2	p_z	0.24
CA1	p_x	0.20

Coordination key:

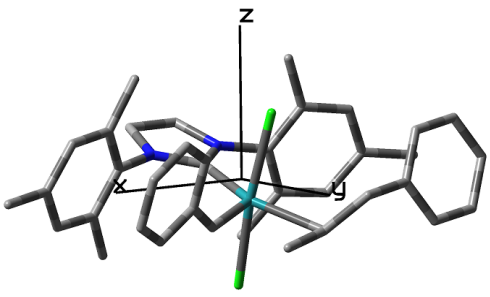

Fig. 23. Reaction state **GA_D2-D3.**

GA_D3

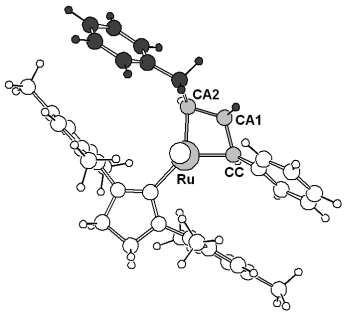

HOMO-15 HOMO-18 HOMO-36 HOMO-59

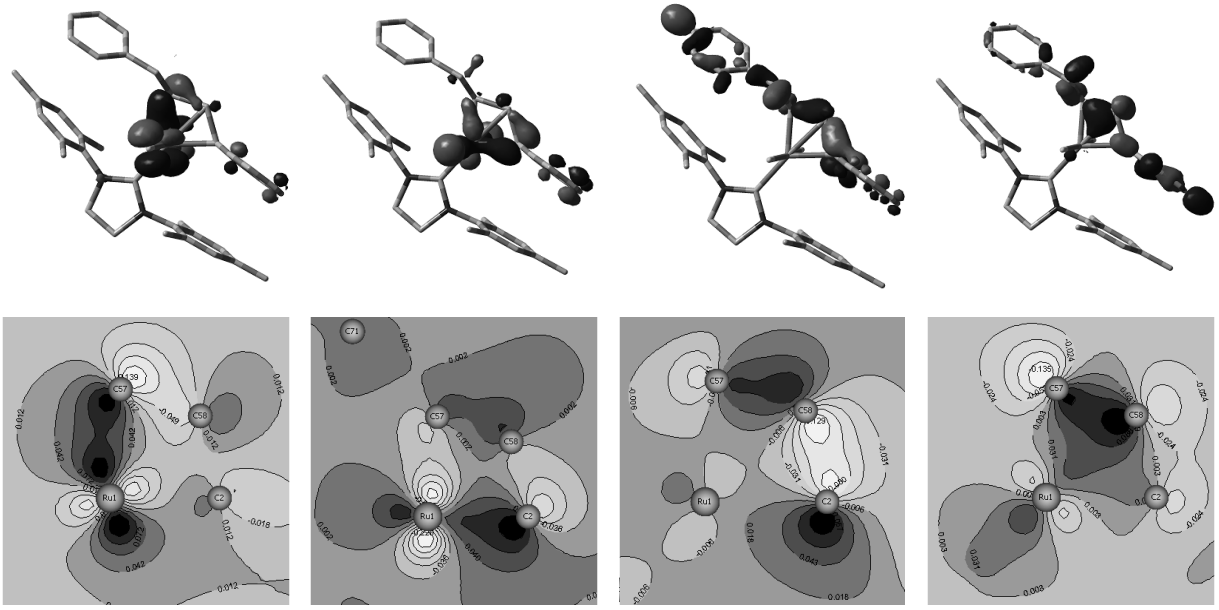

Atom	AO	|coefficient|	Atom	AO	|coefficient|	Atom	AO	|coefficient|	Atom	AO	|coefficient|
Ru	d_{xz}	0.25	Ru	d_{xy}	0.25	CC	p_y	0.22	CA2	p_x	0.22
Ru	$d_{x^2-y^2}$	0.24	CC	p_y	0.21	CA1	p_x	0.21	CA1	p_y	0.22
CA2	p_z	0.21									

Coordination key:

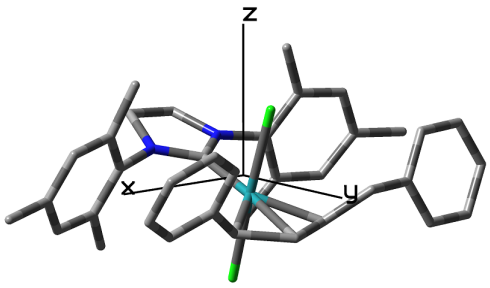

Fig. 24. Reaction state **GA_D3.**

GB_D1

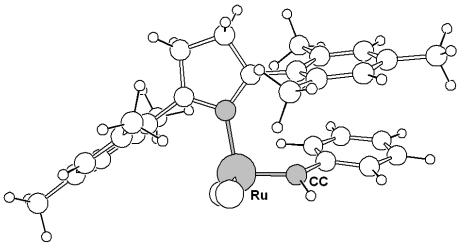

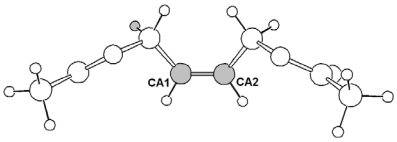

LUMO HOMO

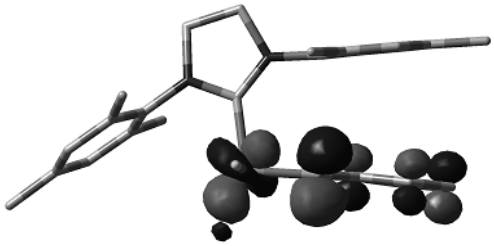

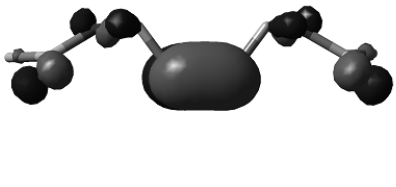

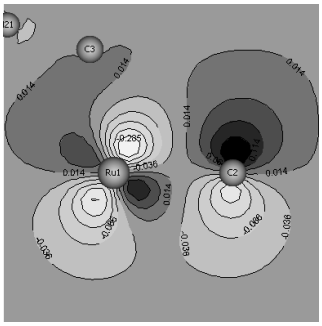

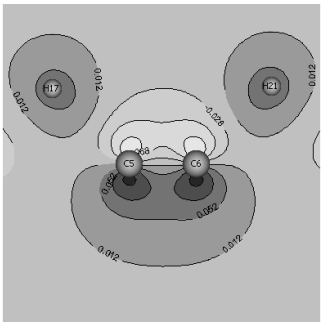

Atom	AO	|coefficient|	Atom	AO	|coefficient|
Ru	d_{xy}	0.44	CA1	p_y	0.41
CC	p_y	0.37	CA2	p_y	0.41
CC	p_y	0.26			
Ru	d_{yz}	0.21			

Coordination key:

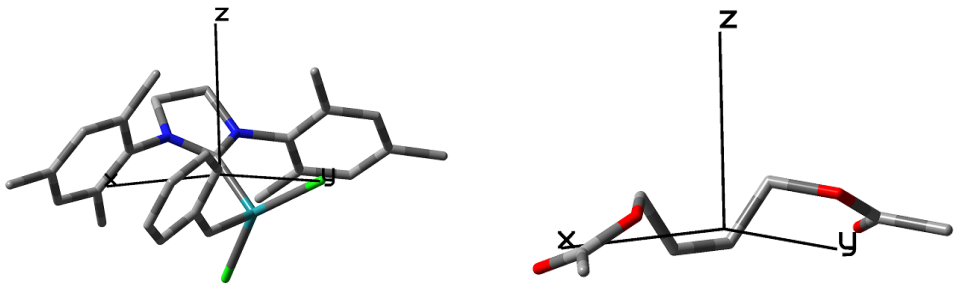

Fig. 25. Reaction state **GB_D1.**

GB_D2-D3

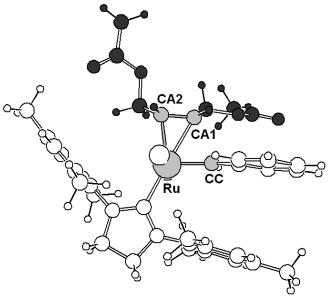

HOMO-16

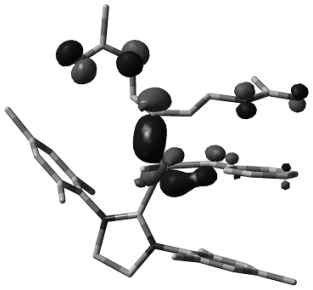

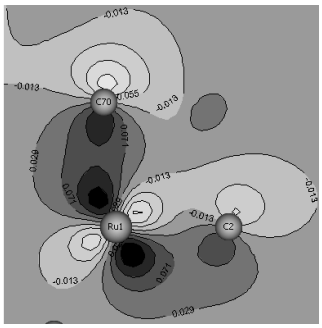

Atom	AO	|coefficient|
CA2	p_y	0.24
Ru	$d_{x^2-y^2}$	0.22
Ru	d_{xy}	0.22

Coordination key:

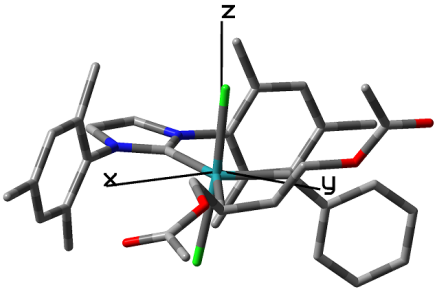

Fig. 26. Reaction state **GB_D2-D3.**

GB_D3

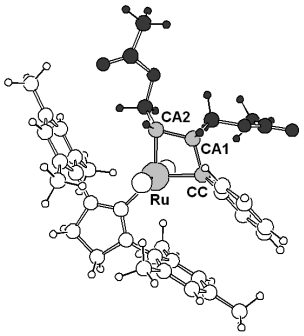

HOMO-19

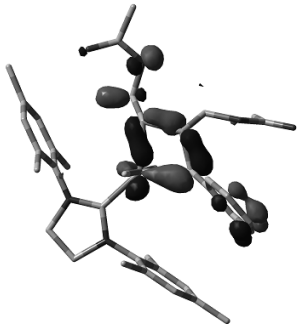

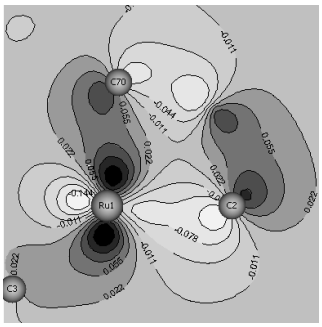

Atom	AO	|coefficient|
Ru	d_{xy}	0.28
CC	p_y	0.24
CA1	p_x	(0.19)
CA2	p_y	(0.17)

Coordination key:

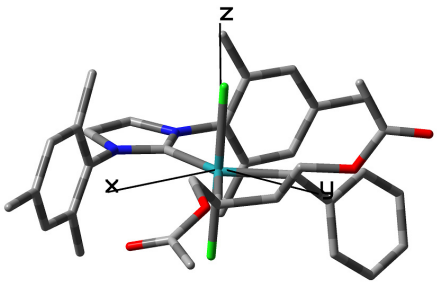

Fig. 27. Reaction state **GB_D3.**

For the reaction energy profiles of **GA** and **GB** (Fig. 28) the dissociation of the ligand is the rate-limiting step. After the dissociation the reaction will run spontaneously to the formation of the metallacyclobutane intermediate. From the graph it is clear that reagent A in the **GA** reaction will bond to the catalyst before reagent B. From the MO diagram of the reactions (Fig. 29) we can see that all the bonding orbitals are lower in energy than the original HOMO. The energy of the bonding orbitals in state **G_D3** indicates a relatively stable metallacyclobutane intermediate, with the **GA** pathway more favored. The value of the orbital gap $|\mathbf{E_H}\text{-}\mathbf{E_L}|$ also points to the fact that the **GA** pathway displayed in the energy profile and the MO diagram with a value of 0.8eV lower than the **GB** pathway are favored.

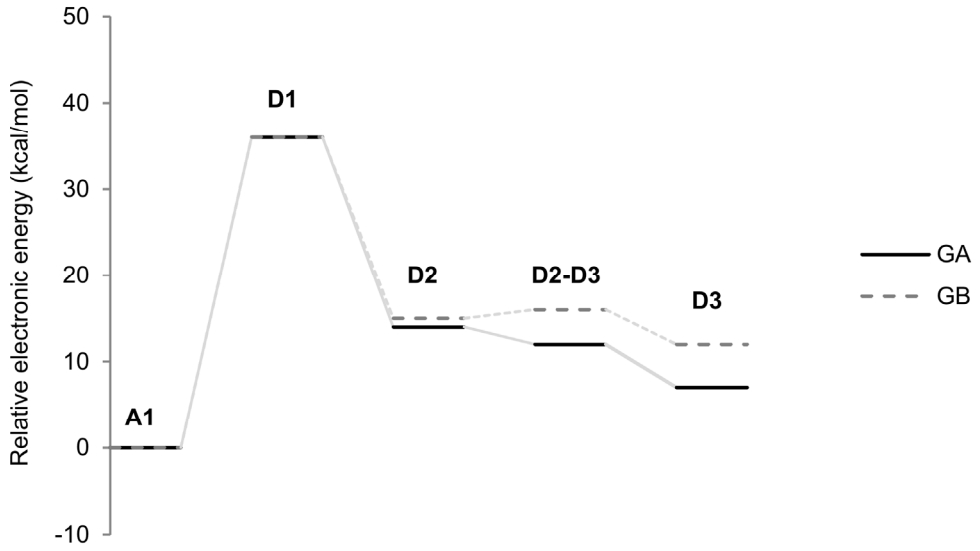

Fig. 28. Relative electronic energy (kcal/mol) reaction profile of alkene(s) with Grubbs carbenes.

The modeling results compare very well with the experimental results. The run was done at 40°C for 12 hours and delivered an 80% yield of cross metathesis product. According to the modeling the metathesis products are favored and fit in well with the Chauvin mechanism.

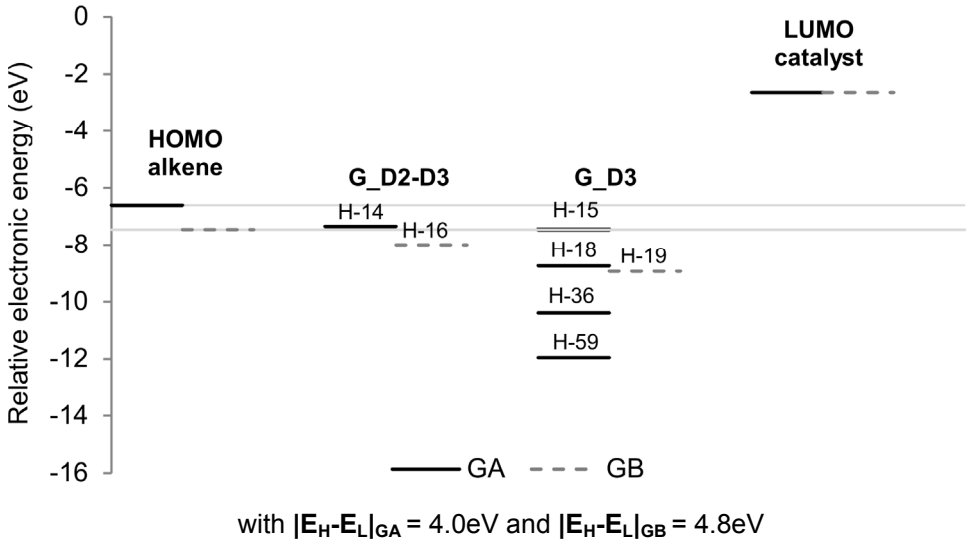

Fig. 29. Partial MO diagram of the bonding MOs of the Grubbs catalyzed reaction.

3.4 Schrock-type metal carbene

According to literature the Schrock carbene follows the associative mechanism pathway [48],[49]. This was also the assumption made for the calculations. In the reaction states **SA_A1** (Fig. 30) and **SB_A1** (Fig. 33) the only major AOC of the LUMO is located on the **Mo**-atom, thus only allowing for primary overlap of the HOMO of the alkene. This may result in a different mechanism than the associative mechanism for Schrock, as we know that the Schrock carbene is a very reactive catalyst. Further reaction steps show the possibility of metathesis products forming but the results are not as clear as in the case of the **Gr2_cat**. In the **SA_A2-A3** (Fig. 31) state the lowest-energy bonding orbital shows bonding between the **Mo**-atom and the **CA1**-atom for the formation of metathesis products, but in the **SB_A2-A3** (Fig.34) the overlap between the **Mo**-atom and the **CA1**-atom is not the lowest-energy bonding orbital. The **SA_A3** (Fig. 32) shows indications of forming further metathesis products seen in the lowest-energy bonding orbital, but none of the other bonding orbitals give any indication of further metathesis products forming. This is also the case in the **SB_A3** (Fig. 35) state where the only bonding orbital, with a AO contribution larger or equal to |0.20|, from the **Mo**-, **CC**-, **CA1**- and **CA2**-atom shows no bonding between the named atoms.

SA_A1

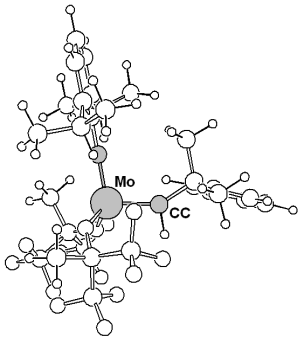

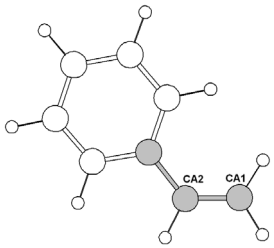

LUMO HOMO

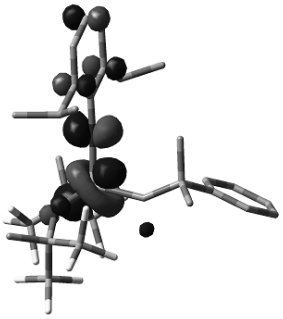

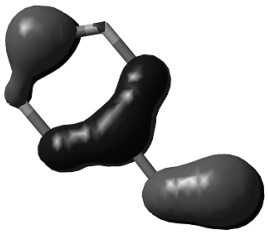

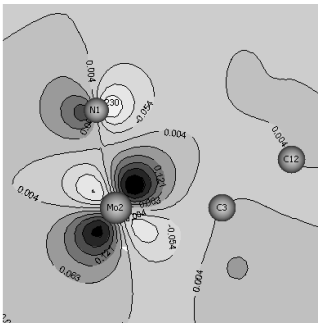

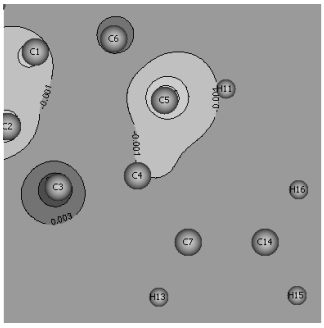

Atom	AO	|coefficient|	Atom	AO	|coefficient|
Mo	d_{xy}	0.50	CA1	p_z	0.38
Mo	d_{yz}	0.35	CA2	p_z	0.26
Mo	d_{xz}	0.33			

Coordination key:

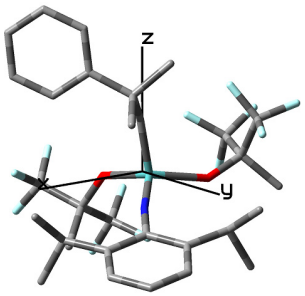

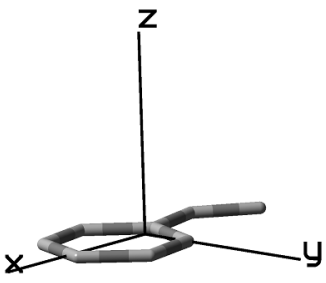

Fig. 30. Reaction state **SA_A1.**

SA_A2-A3

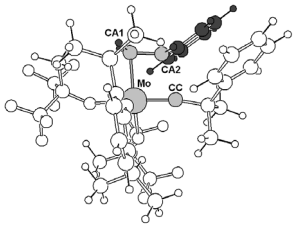

HOMO HOMO-1 HOMO-2 HOMO-15

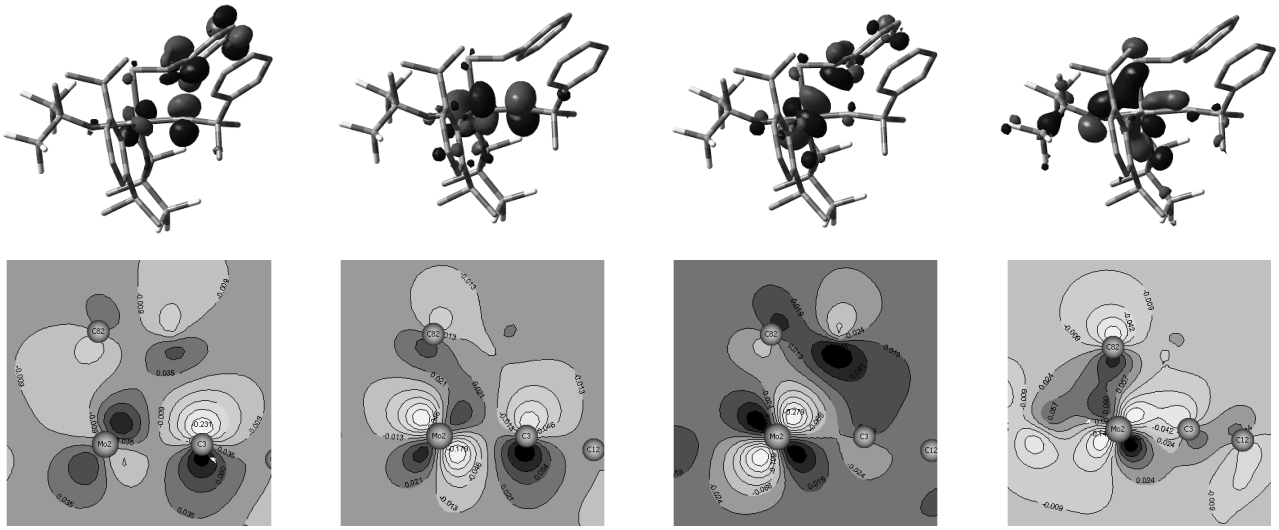

Atom	AO	|coef-ficient|	Atom	AO	|coef-ficient|	Atom	AO	|coef-ficient|	Atom	AO	|coef-ficient|
CC	p_z	0.37	Mo	d_{xy}	0.47	Mo	d_{xz}	0.52	Mo	$d_{z^2-r^2}$	0.25
CC	p_z	0.35	CC	p_y	0.30	Mo	d_{xy}	0.35	CA1	p_z	0.24
Mo	d_{xz}	0.22	Mo	$d_{x^2-y^2}$	0.29	CA2	p_z	0.23	Mo	d_{xz}	0.23
CA2	p_z	0.20	CC	p_x	0.26	Mo	d_{xz}	0.23			
			Mo	$d_{z^2-r^2}$	0.26	Mo	$d_{x^2-y^2}$	0.23			
			Mo	d_{xz}	0.25	CA2	p_z	0.20			
			CC	p_z	0.24						
			CC	p_x	0.24						
			CC	p_y	0.21						
			Mo	d_{xy}	0.20						

Coordination key:

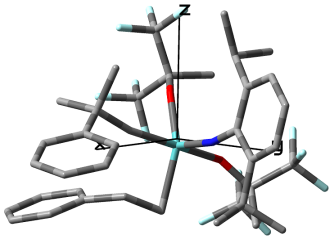

Fig. 31. Reaction state **SA_A2-A3.**

SA_A3

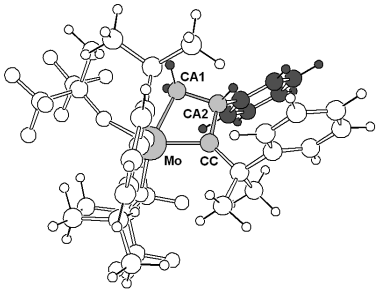

HOMO-2 HOMO-3 HOMO-8 HOMO-16

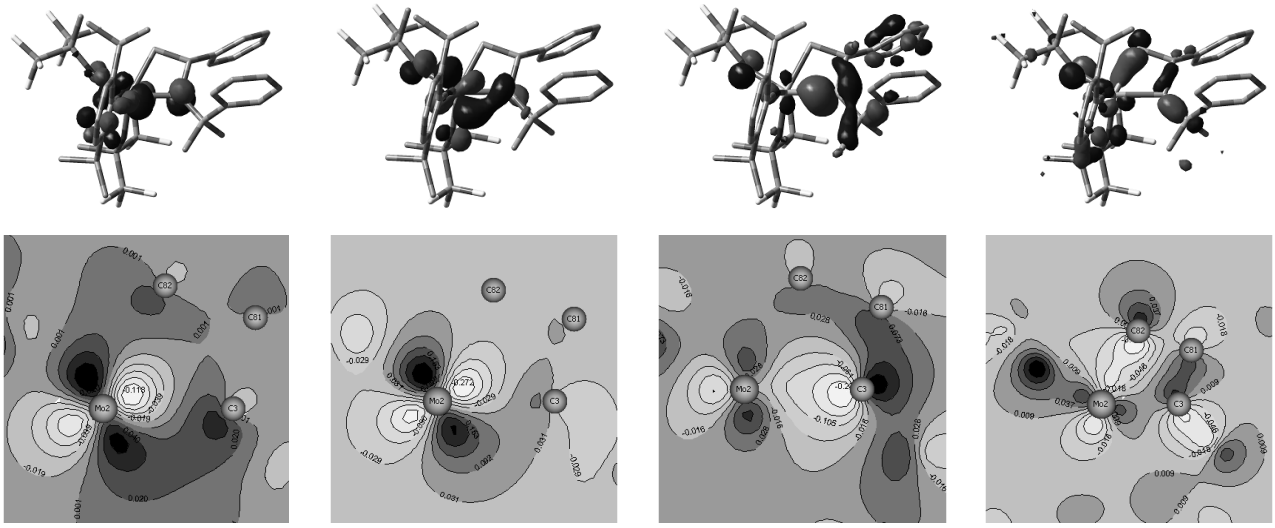

Atom	AO	|coefficient|	Atom	AO	|coefficient|	Atom	AO	|coefficient|	Atom	AO	|coefficient|
Mo	d_{xy}	0.58	Mo	d_{xz}	0.55	CC	p_x	0.37	CA1	p_z	0.20
CC	p_y	0.26	Mo	$d_{z^2-r^2}$	0.46	CC	p_x	0.24	Mo	d_{yz}	0.20
Mo	d_{yz}	0.24	CC	p_y	0.24	Mo	$d_{z^2-r^2}$	0.20			
Mo	d_{xy}	0.20	Mo	d_{yz}	0.21						
Mo	$d_{x^2-y^2}$	0.20									
CC	p_y	0.20									

Coordination key:

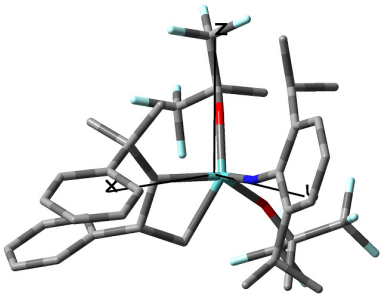

Fig. 32. Reaction state **SA_A3.**

SB_A1

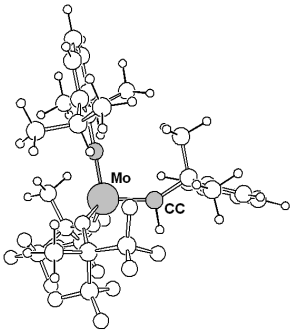

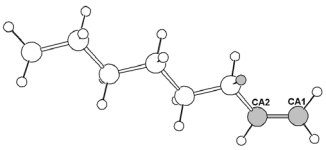

LUMO HOMO

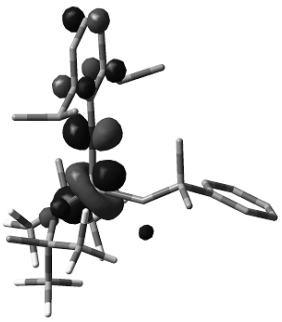

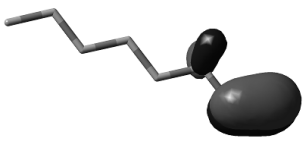

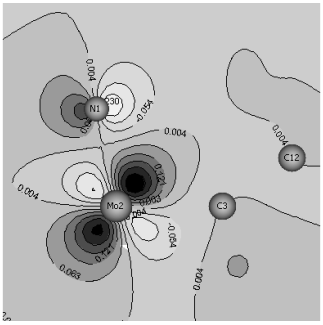

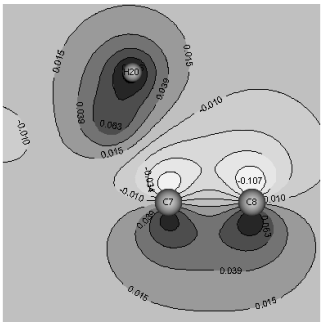

Atom	AO	|coefficient|	Atom	AO	|coefficient|
Mo	d_{xy}	0.50	CA1	p_z	0.49
Mo	d_{yz}	0.35	CA2	p_z	0.44
Mo	d_{xz}	0.33	CA1	p_z	0.20

Coordination key:

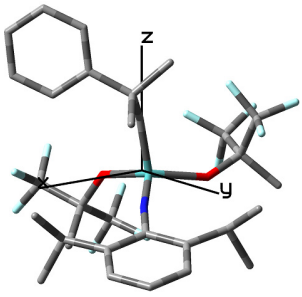

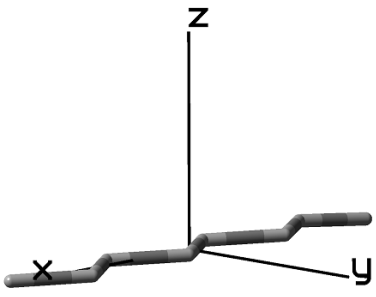

Fig. 33. Reaction state **SB_A1.**

SB_A2-A3

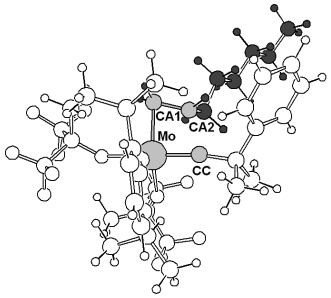

HOMO-1 HOMO-5 HOMO-13 HOMO-16

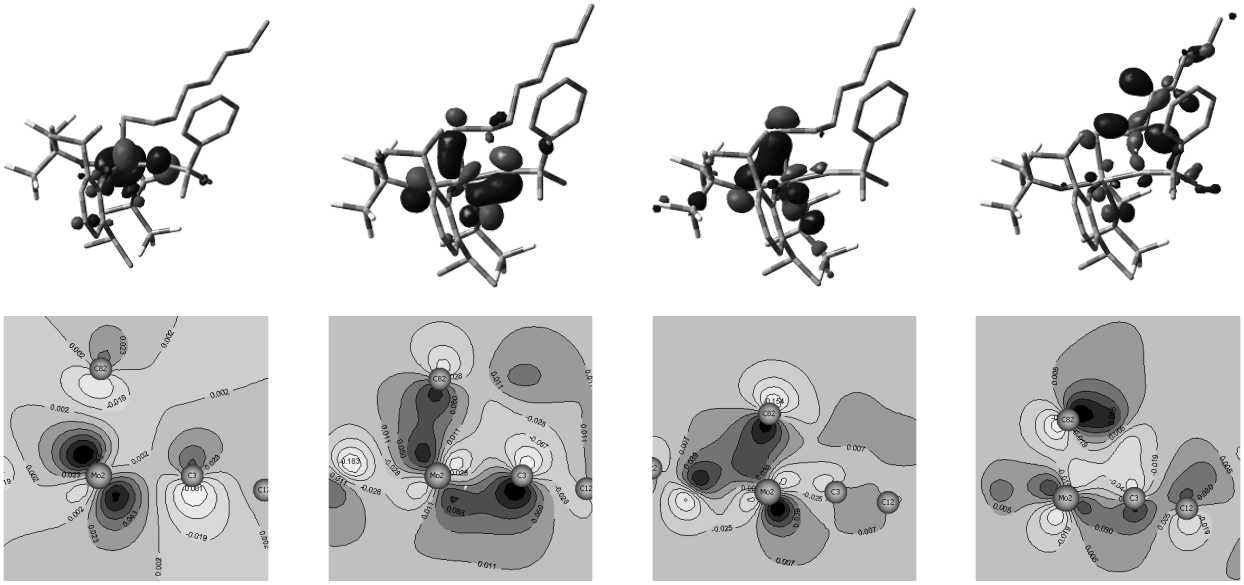

Atom	AO	|coef-ficient|	Atom	AO	|coef-ficient|	Atom	AO	|coef-ficient|	Atom	AO	|coef-ficient|
Mo	$d_{x^2-y^2}$	0.54	Mo	$d_{z^2-r^2}$	0.33	Mo	$d_{z^2-r^2}$	0.25	CA1	p_x	0.22
CC	p_y	0.32	CC	p_z	0.23	CA1	p_x	0.24	CA2	p_z	0.20
Mo	d_{xy}	0.28	CC	p_x	0.21						
CC	p_y	0.27									
Mo	$d_{z^2-r^2}$	0.22									
Mo	$d_{x^2-y^2}$	0.22									
Mo	d_{yz}	0.21									
CC	p_z	0.21									

Coordination key:

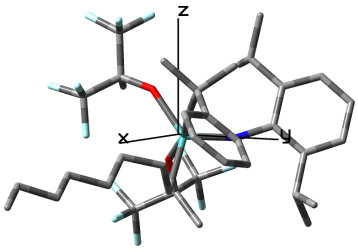

Fig. 34. Reaction state **SB_A2-A3.**

SB_A3

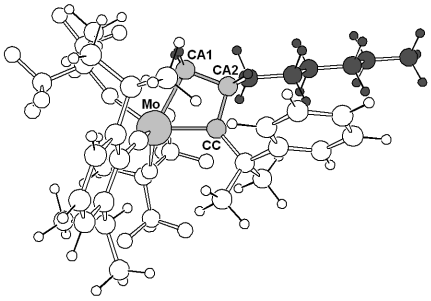

HOMO-2

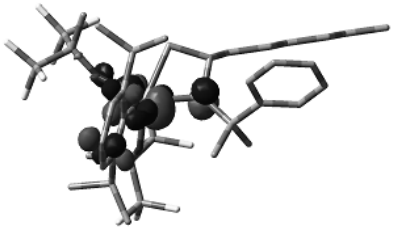

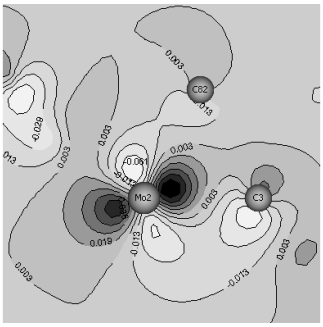

Atom	AO	|coefficient|
Mo	$d_{x^2-y^2}$	0.53
Mo	d_{yz}	0.32
Mo	d_{xy}	0.27
CC	p_y	0.26
CC	p_y	0.22
Mo	$d_{x^2-y^2}$	0.21

Coordination key:

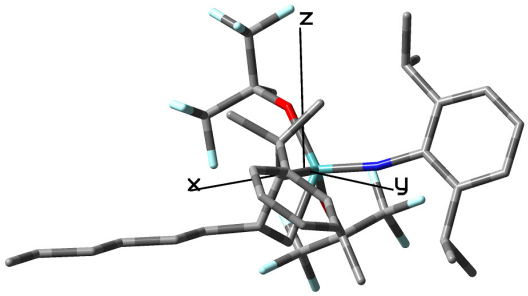

Fig. 35. Reaction state **SB_A3.**

The very high relative energy of the reaction energy profiles of **SA** and **SB** (Fig. 36) clearly indicates a discrepancy in the mechanism of the alkene metathesis reaction catalyzed by the **Mo(Ph)** carbene. This is also seen in the MO diagram (Fig. 37) where more than half of the bonding orbitals have a higher energy than the original HOMO. In Fig. 38 the reaction energy profile trend of Poater *et al.* [19] is compared with the profile of reaction **SA**. To be able to do the comparison, the energy value of reaction state **SA_A2** was matched to the value of the corresponding reaction state in the literature reaction profile [19]. The rest of the reaction steps were then calculated according to the energy gap from **A2**. The reagents of the literature reaction are ethene and a simplified version of **Mo(Ph)** whereas the reagents of reaction **SA** is the true experimental reagents with full complexity. The trend seen in the two reaction profiles is almost similar except for the starting reagents. The difference between the calculated value of state **A2** of Poater *et al.* [19] (0.8 kcal/mol) and the **SA** reaction (408.0 kcal/mol) is 407.2 kcal/mol. From the true reagents it is clear that the proposed mechanism of Chauvin does not fit the metathesis reaction catalyzed by a Schrock metal carbene. The energy values should have been considerably lower if it was taken into account that the experimental reaction was run at a reaction temperature of 25°C and for only 1 hour to give an 89% yield of the cross metathesis product.

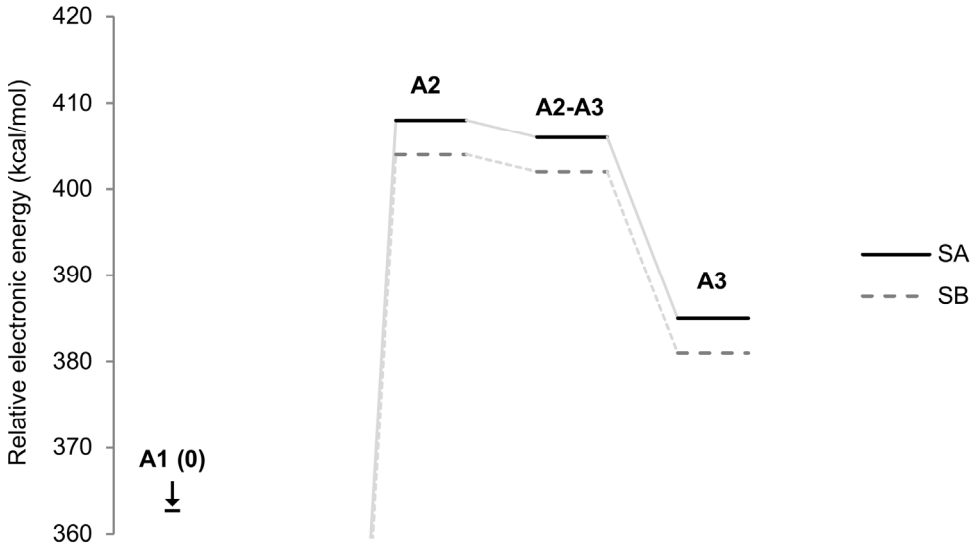

Fig. 36. Relative electronic energy (kcal/mol) reaction profile of alkene(s) with Schrock carbene.

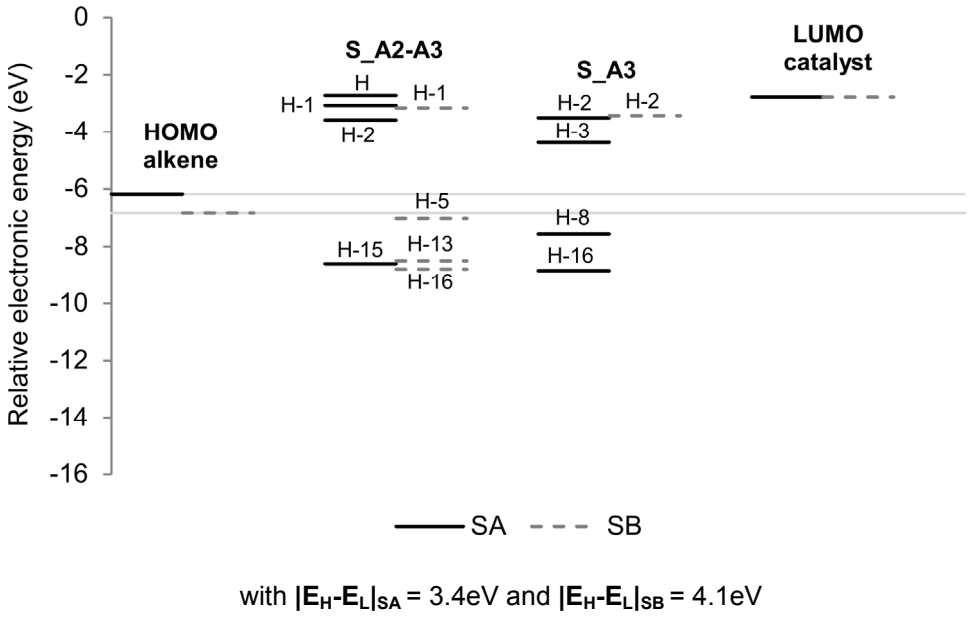

Fig. 37. Partial MO diagram of the bonding MOs of the Schrock catalyzed reaction.

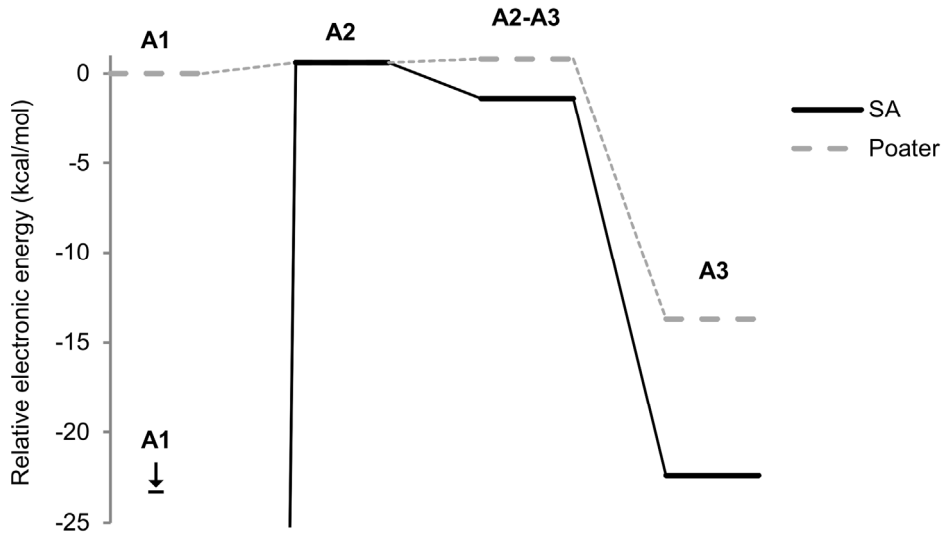

Fig. 38. Comparison between energy profiles of Poater [19] and **SA**.

4. Conclusion

We can conclude that the FMO theory can be used as a chemical reactivity indicator in describing the mechanism of the alkene metathesis reaction in the presence of metal carbenes. Furthermore, the energy and AOCs extracted from the lower lying bonding

orbitals in the MO diagrams give further insight into the formation of the reaction products. In the case of the Fischer-, Tebbe- and Grubbs-type carbene the reactivity could be explained by the modeling results. Only for the Schrock-type carbene the FMO theory could not give a conclusive explanation for the reactivity of the Schrock carbene. We propose further studies need to be done on the mechanism of the alkene metathesis reaction catalyzed by Schrock-type metal carbenes.

References

[1] Y. Chauvin, J. Herisson, Makromol. Chem. 141 (1971) 161.

[2] T.J. Katz, T.H. Ho, N.Y. Shih, Y.C. Ying, V.J. Stuart, J. Am. Chem. Soc. 106 (1984) 2659.

[3] F.N. Tebbe, G.W. Parshall, G.S. Reddy, J. Am. Chem. Soc. 100 (1978) 3611.

[4] S.T. Nguyen, L.K. Johnson, R.H. Grubbs, J. Am. Chem. Soc. 114 (1992) 3974.

[5] R.R. Schrock, J.S. Murdzek, G.C. Bazan, J. Robbins, M. DiMare, M. O'Regan, J. Am. Chem. Soc. 112 (1990) 3875.

[6] C. Adlhart, P. Chen, Angew. Chem. Int. Ed. 41 (2002) 4484.

[7] S.F. Vyboishchikov, M. Bühl, W. Thiel, Chem. Eur. J. 8 (2002) 3962.

[8] S. Fomine, S.M. Vargas, M.A. Tlenkopatchev, Organometallics 22 (2003) 93.

[9] F. Bernardi, A. Bottoni, G.P. Miscione, Organometallics 22 (2003) 940.

[10] L. Cavallo, J. Am. Chem. Soc. 124 (2002) 8965.

[11] C. Costabile, L. Cavallo, J. Am. Chem. Soc. 126 (2004) 9592.

[12] D. Benitez, E. Tkatchouk, W.A. Goddard III, Chem. Commun. (2008) 6194.

[13] C. Adlhart, P. Chen, J. Am. Chem. Soc. 126 (2004) 3496.

[14] M. Vyboishchikov, W. Thiel, Chem. Eur. J. 11 (2005) 3921.

[15] A.C. Tsipis, A.G. Orpen, J.N. Harvey, Dalton Trans. (2005) 2849.

[16] A. Correa, L. Cavallo, J. Am. Chem. Soc. 128 (2006) 13352.

[17] T. Weskamp, F.J. Kohl, W. Hieringer, D. Gleich, W.A. Herrman, Angew. Chem. Int. Ed. 38 (1999) 2416.

[18] T.P.M. Goumans, A.W. Ehlers, K. Lammertsma, Organometallics 24 (2005) 3200.

[19] A. Poater, X. Solans-Monfort, E. Clot, C. Copéret, O. Eisenstein, J. Am. Chem. Soc. 129 (2007) 8207.

[20] W. Janse van Rensburg, P.J. Steynberg, M.M. Kirk, W.H. Meyer, G.S. Forman, J. Organomet. Chem. 691 (2006) 5312.

[21] M. Jordaan, P. Van Helden, C.G.C.E. Van Sittert, H.C.M. Vosloo, J. Mol. Cat. A 254 (2006) 145.

[22] F.T.I. Marx, J.H.L. Jordaan, H.C.M. Vosloo, J. Mol. Model. 15 (2009) 1371.

[23] M. Tlenkopatchev, S. Fomine, J. Organomet. Chem. 630 (2001) 157.

[24] O. Eisenstein, R. Hoffman, J. Am. Chem. Soc. 103 (1981) 5582.

[25] T.R. Cundari, M.S. Gordon, Organometallics 11 (1992) 55.

[26] S.F. Vyboishchikov, M. Bühl, W. Thiel, Chem. Eur. J. 8 (2002) 3962.

[27] C.H. Suresh, N. Koga, Organometallics 23 (2004) 76.

[28] B.F. Straub, Angew. Chem. Int. Ed. 44 (2005) 5974.

[29] B.F. Straub, Adv. Synth. Catal. 349 (2007) 204.

[30] G. Occhipinti, H. Bjørsvik, V.R. Jensen, J. Am. Chem. Soc. 128 (2006) 6952.

[31] R.L. Lord, H. Wang, M. Vieweger, M. Baik, J. Organomet. Chem. 691 (2006) 5505.

[32] I. Fernández, N. Lugan, G. Lavigne, Organometallics 31 (2012) 1155.

[33] M. Vasiliu, S. Li, A.J. Arduengo III, D.A. Dixon, J. Phys. Chem. C. 115 (2011) 12106.

[34] E. Folga, T. Ziegler, Organometallics 12 (1993) 325.

[35] H.H. Fox, M.H. Schofield, R.R. Schrock, Organometallics 13 (1994) 2804.

[36] J.I. Du Toit, A modelling investigation into the mechanism of the homogeneous alkene metathesis reaction, NWU (Potchefstroom), (M.Sc. – dissertation), 2009. URL: http://hdl.handle.net/10394/4408.

[37] J.I. Du Toit, C.G.C.E. Van Sittert, H.C.M. Vosloo, J. Organomet. Chem. (2012) Submitted (Chapter 3 Article in thesis).

[38] (a) I. Fleming, Frontier Orbitals and Organic Chemical Reactions. WILEY, Chichester, 1976.; (b) I. Fleming, Molecular Orbitals and Organic Chemical Reactions, Reference Ed. WILEY, Chichester, 2010.

[39] C.P. Casey, H.E. Tuinstra, M.C. Saeman, J. Am. Chem. Soc. 98 (1976) 608.

[40] F.N. Tebbe, G.W. Parshall, D.W. Ovenall, J. Am. Chem. Soc. 101 (1979) 5074.

[41] A.K. Chatterjee, T. Choi, D.P. Sanders, R.H. Grubbs, J. Am. Chem. Soc. 125 (2003) 11360.

[42] W.E. Crowe, Z.J. Zhang, J. Am. Chem. Soc. 115 (1993) 10998.

[43] Accelrys Software Inc, Materials Studio Modeling Environment, Release 5.0.0.0. San Diego, Accelrys Software Inc, 2009.

[44] M.J. Frisch, G.W. Trucks, H.B. Schlegel *et al.*, Gaussian 03, Revision B.03. Gaussian Inc, Pittsburgh PA, 2003.

[45] S. Leonid, Chemissian Version 2.000, 2005-2011.

[46] L.J. Farrugia, J. Appl. Crystallogr. 30 (1997) 565.

[47] F.Z. Dörwald, Metal Carbenes in Organic Synthesis. Wiley-VCH, Weinheim, 1999.

[48] R.R. Schrock, A.H. Hoveyda, Angew. Chem. Int. Ed. 42 (2003) 4592.

[49] R.R. Schrock, Chem. Rev. 109 (2009) 3211.